Partial prion cross-seeding between fungal and mammalian amyloid signaling motifs

Thierry Bardin[1], Asen Daskalov[1], Sophie Barrouilhet[1*], Alexandra Granger-Farbos[1], Bénédicte Salin[1], Corinne Blancard[1], Sven J. Saupe[1#] and Virginie Coustou[1#]

[1] Non-Self Recognition in Fungi, Institut de Biochimie et de Génétique Cellulaire (CNRS UMR 5095, Université de Bordeaux), 33077 Bordeaux, France.

[*] Current Address: Universite de Pau et des Pays de l'Adour, E2S UPPA, CNRS, IPREM UMR 5254, Hélioparc, 64053 Pau, France

[#]Corresponding authors

E-mail: virginie.coustou@ibgc.cnrs.fr (VC); sven.saupe@ibgc.cnrs.fr (SJS)

Running title: Amyloid signaling pathways in *P. anserina*

Key words: amyloid; prion; programmed cell death; RHIM; RIP1, RIP3

Abstract

In filamentous fungi, NLR-based signalosomes activate downstream membrane-targeting cell-death inducing proteins by a mechanism of amyloid templating. In the species *Podospora anserina*, two such signalosomes, NWD2/HET-S and FNT1/HELLF have been described. An analogous system, involving a distinct amyloid signaling motif termed PP was also identified in the genome of the species *Chaetomium globosum* and studied using heterologous expression in *Podospora anserina*. The PP-motif bears resemblance to the RHIM and RHIM-like motifs controlling necroptosis in mammals and innate immunity in flies. We identified here, a third NLR signalosome in *Podospora anserina* comprising a PP-motif and organized as a two-gene cluster encoding a NLR and a HELL-domain cell-death execution protein termed HELLP. We show that the PP-motif region of HELLP forms a prion we term [π] and that [π] prions trigger the cell-death inducing activity of full length HELLP. We detect no prion cross-seeding between HET-S, HELLF and HELLP amyloid motifs. In addition, we find that akin to PP-motifs, RHIM motifs from human RIP1 and RIP3 kinases are able to form prions in *Podospora*, and that [π] and [Rhim] prions partially cross-seed. Our study shows that *Podospora anserina* displays three independent cell-death inducing amyloid signalosomes. Based on the described functional similarity between RHIM and PP, it appears likely that these amyloid motifs constitute evolutionary related cell-death signaling modules.

Importance

Amyloids are β-sheet-rich protein polymers that can be pathological or display a variety of biological roles. In filamentous fungi, specific immune receptors activate programmed cell-death execution proteins through a process of amyloid templating akin to prion propagation.

41 Among these fungal amyloid signaling sequences, the PP-motif stands out because it shows
42 similarity to RHIM, an amyloid sequence controlling necroptotic cell-death in mammals. We
43 characterized an amyloid signaling system comprising a PP-motif in the model species
44 *Podospora anserina* thus bringing to three the number of independent amyloid signaling cell
45 death pathways described in that species. We then show that human RHIM motifs not only
46 propagate as prions in *P. anserina* but also partially cross-seed with fungal PP-prions. These
47 results indicate that in addition to show sequence similarity, PP and RHIM-motif are at least
48 partially functionally related, supporting a model of long-term evolutionary conservation of
49 amyloid signaling mechanisms from fungi to mammals.
50

51 # Introduction

52 Prions are protein polymers that behave as infectious entities by propagating their
53 amyloid structural state (1, 2). In addition to disease causing prions in mammals, prions have
54 been identified in fungi as infectious, cytoplasmic, non-mendelian genetic elements (3). One
55 such prion is [Het-s] of the filamentous fungus *Podospora anserina.* [Het-s] functions in a non-
56 self recognition process known as heterokaryon incompatibility. The *het-s* gene exists as two
57 incompatible allelic variants termed *het-s* and *het-S*. The HET-s protein when assembled into
58 the self-propagating prion form confers incompatibility to the HET-S variant. Co-expression of
59 the [Het-s] prion with HET-S leads to cell death. At the macroscopic level, the incompatibility
60 reaction leads to the formation of an abnormal contact line between the strains termed
61 "barrage". The soluble non-prion form confers a phenotype termed [Het-s*] compatible with
62 HET-S (4, 5). [Het-s*] strains acquire the prion state either spontaneously at a low frequency
63 or systematically after fusion with a prion infected strain. HET-s and HET-S are highly
64 homologous allelic variants that display two domains, a C-terminal Prion-Forming Domain
65 (PFD) necessary and sufficient for prion propagation and a N-terminal α-helical globular
66 domain named HeLo responsible for cell-death inducing activity (6, 7). The HET-s PFD is
67 natively unfolded in the soluble state and upon prion formation assembles into to a specific
68 cross-β amyloid structure (6, 8–10). The HET-s β-solenoid fold is composed of 2 rungs of β-
69 strands per monomer, comprising two 21 amino acid long imperfect repeats (R1 and R2)
70 connected by a flexible loop (9, 11). In [Het-s]/HET-S incompatibility cell death is triggered
71 when the [Het-s] PFD templates conversion of the HET-S PFD region into the β-solenoid fold
72 which in turn induces refolding of the HET-S HeLo domain that acquires pore-forming activity
73 by exposing an N-terminal transmembrane helix targeting the cell membrane (7, 12). In this

74 incompatibility system, HET-S acts as cell-death execution protein and [Het-s] triggers its
75 activation.

76 Further work on the [Het-s] system revealed that this incompatibility system is
77 evolutionary derived from a programmed cell death (PCD) pathway in which HET-S is activated
78 by a specific NLR (Nod-like receptor) (13). NLR receptors are intracellular receptors that
79 control immune defense and PCD pathways in animals, plants and fungi and function by ligand
80 induced oligomerization (14, 15). The NWD2 NLR receptor is encoded by the gene immediately
81 adjacent to *het-S* in the *P. anserina* genome and displays a central NACHT nucleotide binding
82 and oligomerization domain and a C-terminal WD40 repeat domain. The N-terminal region of
83 NWD2 displays a short region of homology to the R1 and R2 motifs of HET-s. This region
84 designated R0 is able to adopt a *het-s*-like fold. Ligand induced oligomerization of NWD2
85 allows for spatial clustering of R0 motifs, cooperative nucleation of the β-solenoid fold which
86 then templates conversion of the homologous domain in HET-S and activation of the HeLo
87 domain (13, 16, 17). More generally, it is proposed that a fraction of the NLR receptors in fungi
88 activate their cognate effector domains by a mechanism of prion amyloid templating by which
89 the amyloid fold formed after oligomerization of the NLR receptor is transmitted through
90 heterotypic interactions to the amyloid motif found in the C-terminal of the effector protein
91 (18). NWD2/HET-S pair was used as a paradigm in bioinformatic screens to identify additional
92 NLR/effector pairs functioning through amyloid templating in fungi (16, 19). These approaches
93 resulted in particular in the identification of five *het-s*-related amyloid motifs families (HRAMs)
94 and in the characterization in *Podospora anserina* of a distant homolog of HET-S termed HELLF
95 and belonging the HRAM5 family (20). HELLF encodes a protein with a HeLo-like N-terminal
96 domain and a C-terminal PFD with two repeated submotifs that share only 17% identity to the
97 HET-s PFD. The HeLo-like domain shows distant homology to the HET-S HeLo domain but also

98 to the 4HB pore-forming domain of the MLKL protein (21), the terminal effector protein of
99 necroptotic death in mammals, which led to the proposition that this form of fungal PCD is
100 related to mammalian necroptosis (22). The gene adjacent to *hellf* encodes a NLR with a NB-
101 ARC domain and TPR repeats termed FNT1, which bears an N-terminal R0 region homologous
102 to the HELLF R1 and R2 PFD repeats. HELLF behaves analogously to HET-S in every aspect that
103 was analyzed. The C-terminal region of HELLF forms a prion termed [Φ] and [Φ] is
104 incompatible with full length HELLF. Upon interaction with [Φ], HELLF relocates to cell
105 membrane region and causes cell death. The N-terminal region of FNT1 forms fibrils and is
106 able to induce [Φ] prion formation. The solid-state NMR structure of the HELLF PFD structure
107 revealed that HET-s and HELLF prions have an almost identical backbone structure in spite of
108 extensive sequence divergence. The FNT1/HELLF system thus constitutes a second cell death-
109 inducing amyloid signaling pathway of *Podospora anserina*. Noteworthy is the fact that in spite
110 of their almost identical backbone structure [Het-s] and [Φ] prions do not cross-seed
111 indicating that NWD2/HET-S and FNT1/HELLF constitute two parallel signaling pathways.

112 In bioinformatics surveys, additional amyloid signaling motifs were identified in other
113 fungi (14, 16). In particular, a prion motif termed PP was identified in the genome of
114 *Chaetomium globosum* in a three-gene cluster and functionally studied using heterologous
115 expression in *Podospora anserina*. In this specific case, the NLR termed PNT1 regulates
116 activation of two effector proteins, a HeLo-like domain cell-death inducing protein termed
117 HELLP and a putative lipase, SBP (renamed herein CgHELLP, CgPNT1 and CgSBP for clarity).
118 The PP-motif is related in sequence to the RHIM amyloid motif that controls assembly of the
119 RIP1 and RIP3 kinases in the necroptosis pathway in mammals (13, 22, 23). RHIM-like amyloid
120 motifs also occurs in the PGRP-LC, PGRP-LE, and Imd proteins controlling anti-bacterial
121 immunity in Drosophila (24). The structure of the mammalian RIP1-RIP3 core (forming an

122 hetero-amyloid signaling complex) has recently been established (25). RHIM amyloids
123 comprise two protein units per cross-β layer that run antiparallel and are interdigitated in a
124 compact hydrophobic interface formed by the core G-(I,V)-Q-(I,V)-G motif. This central core
125 motif is common to the PP-motif but in absence of structural characterization of PP-amyloids,
126 it cannot at present be ascertained that this short sequence homology reflects structural
127 similarity between RHIM and PP-amyloids.

128 Herein, we mine the genome of *P. anserina* and identify HELLP, a novel PP-motif protein
129 that defines, in that species, a third cell-death inducing amyloid signaling pathway comprising
130 the HELLP cell-death execution protein and a NLR (PNT1). We show that the C-terminal PP-
131 motif of HELLP (HELLP(214-271)) forms a prion termed [π] in *Podospora anserina* and
132 assembles into fibrils *in vitro.* We find that akin to HET-S and HELLF, cell-death inducing activity
133 of HELLP is activated by [π] prions formed by HELLP(214-271) or by the N-terminal region of
134 PNT1, PNT1(1-31). We analyze in *Podospora anserina* the functional interactions of the HET-
135 s, HELLF and HELLP PFD prions and find that they form three independent signaling systems.
136 We further analyze prion formation by human RHIM motifs from RIP1 and RIP3 kinases and
137 find that [Rhim] and [π] prions partially cross-seed underlying the functional similarity
138 between these mammalian and fungal amyloid motifs.

139

140 # Results

141 ## A PP-motif gene cluster in *Podospora anserina*

142 During the course of a survey of NLR encoding genes in fungi, we identified in
143 *Podospora anserina,* a gene encoding a NLR with a NB-ARC domain and TPR repeats
144 (*Pa_5_8060,* PNT1), (14). We found after manual re-annotation, that the adjacent gene

145 (*Pa_5_8070*) encodes a HeLo-like domain protein, we term HELLP (Fig. 1A). HELLP shows 56 %
146 similarity to the CgHELLP cell-death execution protein of *Chaetomium globosum* (Fig. 1B and
147 Fig. S1) (22). As previously reported for CgHELLP and HELLF, the HELL domain of HELLP shows
148 homology to the 4HB membrane-targeting domain of the mammalian MLKL necroptosis
149 execution protein (Fig. S1). The N-terminal region of PNT1 and the C-terminal region of HELLP
150 share a region of homology encompassing a predicted PP-amyloid motif (Fig. 1B) (22). This
151 region is also homologous to the RHIM motif found in the RIP1 and RIP3 kinases in humans
152 (23, 25). Based on the resemblance with the PP gene-cluster of *C. globosum*, we reasoned that
153 after *nwd2/het-s* and *fnt1/hellf*, the *pnt1/hellp* gene pair might encode the components of a
154 third amyloid NLR signalosome in Podospora (Fig. 1A). We thus engaged into the functional
155 characterization of this gene pair.
156

157 **The C-terminal region of HELLP is a prion-forming domain**

158 In order to analyze whether the C-terminal region of HELLP displays the anticipated prion
159 forming ability, we generated different constructs with the C-terminal domain of HELLP (214-
160 271) fused either to GFP or RFP (in a C-terminal position) or to GFP in an N-terminal position.
161 These constructs were expressed in a *Δhellp* strain of *P. anserina*. For the different constructs,
162 a population of 25 to 47 distinct transformants was analyzed by fluorescence microscopy. We
163 observed either dot-like or diffuse fluorescence (Fig. 1C). The fraction of transformants
164 exhibiting dot-like fluorescence was found to increase with growth duration (Table 1). The
165 highest rate of foci formation was observed for the fusion protein bearing the GFP in N-
166 terminal position. Within 19 days, all tested GFP-HELLP(214-271) transformants, displayed
167 fluorescent foci. For all three fusion constructs, strains with diffuse fluorescence were
168 systematically converted to the foci phenotype after cytoplasmic contact with strains

169 expressing foci (Table 1), indicating that the foci state is transmitted by cytoplasmic contact
170 and infectious. By analogy with the [Het-s] system, we term the phenotypic state with diffuse
171 fluorescence [π*] and the foci state [π] (Fig. 1C). We conclude from these experiments that
172 the PP-motif region of HELLP(214-271) allows for prion formation and propagation. To
173 determine whether as previously described for [Het-s] (26), the [π] state could be reverted to
174 [π*] in meiotic progeny, we analyzed 40 progeny of a *Δhellp Δhet-s Δhellf GFP-hellp(214-271)*
175 [π] x *Δhellp Δhet-s Δhellf het-s-RFP* cross. Among the 20 progeny containing the *GFP-hellp(214-*
176 *271)* transgene, three displayed a [π*] phenotype, indicating that akin to [Het-s], the [π] prion
177 can be cured in sexual crosses.

178 A larger construct, with HELLP(171-271) fused to GFP either in N- or C-terminus also led
179 to foci formation (Fig. S2A) but in contrast to analogous HET-S and CgHELLP constructs (HET-
180 S(157-289)-GFP and CgHELLP(170-278)-GFP), HELLP(171-271) fusions did not form elongated
181 aggregates (22, 27).

182 The HELLP(214-271) PFD region was also expressed in *E. coli* with a C-terminal histidine
183 tag and purified under denaturing conditions. Upon removal of the denaturant by dialysis, the
184 protein spontaneously formed fibrils that often associated laterally as bundles (Fig. 1D).

185

186 [π] prions triggers incompatibility upon interaction with full-length HELLP

187 It was shown that HET-S, HELLF and CgHELLP cell-death inducing activity is triggered by
188 interaction with the prion form of their respective PFDs (7, 12, 20, 22). As a result,
189 confrontation of strains expressing PFDs in the prion state with strains expressing the
190 corresponding full-length protein leads to an incompatibility reaction which results in death
191 of the fusion cells and, at the macroscopic level, in formation of an abnormal contact line

192 termed barrage (20, 22, 27, 28). To determine whether HELLP could also determine
193 incompatibility, strains expressing GFP-HELLP(214-271) were confronted to strains expressing
194 full-length HELLP, either from the wild-type resident copy or from HELLP-GFP or HELLP-RFP
195 transgene copies (in a *Δhellp* background) (Fig. 2A). A barrage reaction was observed
196 systematically and specifically in confrontations with strains expressing the [π] phenotype (as
197 determined by presence of foci). [π*] strains did not produce a barrage reaction. 24
198 transformants were analyzed in parallel for barrage formation and presence of foci and the
199 two phenotypes were strictly correlated. The barrage reaction was stronger with strains
200 expressing HELLP-GFP or -RFP fusions from the strong *gpd* promoter than with strains
201 expressing HELLP from the resident copy as shown in Fig. 2A. We verified that at the
202 microscopic level, barrage formation was indeed associated with cell death using the vital dye
203 methylene blue (Fig. S4).

204 As expected the barrage formation phenotype was transmitted by cytoplasmic contact.
205 Upon contact with barrage forming strains, a compatible strain invariably became capable of
206 forming a barrage with a strains expressing full length HELLP (Tables S1 and also S2 to S6, Fig.
207 S2). Based on these experiments the definition of the [π] phenotype can be expanded to
208 represent both the foci state of the PP-motif GFP and RFP fusions and the ability to produce a
209 barrage reaction to full-length HELLP. The [π*]/[π] phenotypes of HELLP(214-271) are in that
210 sense analogous to [Het-s*]/[Het-s] phenotypes of HET-s (4) and [Φ*]/[Φ] phenotypes of
211 HELLF(209-277) (20).

212 It was shown that prion conversion of the HET-S PFD leads to the refolding of the HET-S
213 HeLo domain that acquires pore-forming activity by exposing its N-terminal transmembrane
214 helix, relocating it to the cell membrane and inducing cell death (7, 12). The same
215 relocalization process was previously observed for HELLF and CgHELLP in the incompatibility

216 reaction leading to cell death (20, 22). We thus determined whether HELLP relocates in the
217 cell membrane region upon interaction with [π] prions. We examined the contact zone
218 between incompatible [π] and HELLP-GFP or -RFP expressing strains (Fig. 2B). While full length
219 HELLP-GFP or -RFP alone yield a diffuse fluorescence signal that remains stable over time (Fig.
220 S3), in fusion cells co-expressing these proteins and the prion form of HELLP(214-271)-RFP or
221 GFP-HELLP(214-271), we observed a relocalization of HELLP in the vicinity of the cell
222 membrane region. We conclude that in these experiments, HELLP behaves as previously
223 described for HET-S, HELLF and CgHELLP and locates in the cell membrane region in fusion
224 cells. Further experiments are required to determine whether HELLP directly interacts with
225 the membrane and if so how this interaction causes cell death.
226

227 **The PNT1(1-31) region forms a prion and induces HELLP activation**

228 It has been shown that the N-terminal region of NWD2 adopts an amyloid fold, displays
229 prion infectivity and is able to activate HET-S pore-forming activity (13). Similarly, N-terminal
230 regions of the FNT1 and CgPNT1 NLRs behave as PFDs and trigger cell-death inducing activity
231 of their cognate effectors proteins, HELLF and CgHELLP respectively (22). To determine
232 whether the N-terminal region of PNT1 displays similar properties, we expressed PNT1(1-31)
233 fused to GFP or RFP in *Δhellp* strains. Two phenotypic states were observed, a diffuse
234 cytoplasmic fluorescence state, and a foci state analogous to the [π∗] and [π] phenotypes
235 observed previously with HELLP(214-271) (Fig. 3A). Spontaneous conversion to the foci form
236 occurred upon prolonged subculture (Table 1) and cytoplasmic contact with foci-containing
237 strain induced systematic conversion to the foci state (Table 1). PNT1(1-31)-GFP strains with
238 fluorescent foci produced a barrage reaction to strains expressing full length HELLP (not

239 shown). PNT1(1-31)-GFP [π] strains systematically convert [π*] HELLP(214-271)-RFP strains to
240 the [π] state. Conversely, [π] HELLP(214-271)-RFP systematically convert [π*] PNT1(1-31)-GFP
241 to the [π] state (Table S2).

242 PNT1(1-31) and HELLP(214-271) were then co-expressed in the same strain (Fig. 3B).
243 Fluorescence was either diffuse for both HELLP(214-271)-RFP and PNT1(1-31)-GFP or dot-like
244 concomitantly for the two proteins. Cells in which one of the proteins formed foci while the
245 other remained diffuse were not observed (Fig. 3B, Table S7). HELLP(214-271)-RFP and
246 PNT1(1-31)-GFP dots generally co-localized (Fig. 3B, Table S8). The same was true during co-
247 expression of PNT1(1-31)-RFP and GFP-HELLP(214-271). An initial diffuse state could however
248 not be observed in this setting presumably as the result of the high spontaneous conversion
249 rate of the N-terminal GFP-HELLP(214-271) fusion protein (Table 1).

250 Finally, we observed fusion cells between strains expressing PNT1(1-31) in the [π] state
251 and strains expressing full-length HELLP (Fig. 3C, Fig. S4). We observed the relocalization of
252 HELLP to the plasma membrane region and cell death of the fusion cells. Thus, consistent with
253 the proposed role of HELLP as cell death execution protein activated by the PNT1 NLR, we find
254 that the PP-motif region of PNT1 forms a prion and is able to activate HELLP.

255

256 HET-S, HELLF and HELLP are components of three independent cell-death 257 inducing pathways

258 We recently reported the lack of cross-seeding between [Het-s] and [Φ] prions indicating
259 the existence of two independent parallel amyloid signaling pathways in *P. anserina* (20).
260 Here, we identify HELLP as an effector in a third amyloid signaling pathway in *P. anserina* and
261 therefore wanted to analyze potential cross-interaction between these pathways. We

262 analyzed [π*] conversion by [Het-s] and [Φ] prions (Table S3). Strains expressing HELLP(214-
263 271)-GFP or -RFP and displaying the [π*] phenotype were confronted to strains expressing [π],
264 [Φ] or [Het-s] prions and then tested for their ability to form a barrage with tester strains
265 expressing full-length HELLP. Barrage were observed only (and systematically) when the prion
266 donor strain expressed [π] prions indicating that [π*] conversion does not occur in presence
267 of [Het-s] or [Φ] prions.

268 We also analyzed the cross-activation of the cell-death effectors of the three systems by
269 the different prions (Table S4). We used incompatibility assays and confronted [π], [Φ] or [Het-
270 s] prion expressing strains with strains expressing either HELLP, HELLF or HET-S full-length
271 proteins. We observed barrage formation solely when [π] strains were confronted with HELLP
272 expressing strains, [Φ] with HELLF and [Het-s] with HET-S, that is, uniquely when the prion and
273 the effector bear the same PFD. We observe no cross-interaction between these three
274 amyloid signaling pathways.

275 To further analyze HELLP/HELLF and HELLP/HET-s interactions, we co-expressed
276 HELLP(214-271) with either HET-s or HELLF(209-271) in a *Δhellp Δhet-s Δhellf* strain. We
277 observed the diffuse and foci states co-existing in all possible combinations (Fig. 4, Fig S5, and
278 Table S7). Namely, strains expressing HELLP(214-271) and HET-s could display four different
279 phenotypes: [Het-s]/[π] and [Het-s*]/[π*] but also [Het-s]/[π*] and [Het-s*]/[π]. The same was
280 true for HELLP(214-271) and HELLF(209-277) co-expression (Fig. 4, S5 and Table S7). These
281 results are consistent with the conversion experiments and show that [Φ] or [Het-s] prions do
282 not efficiently convert [π*] and conversely that [π] prions do not efficiently convert [Φ*] or
283 [Het-s*]. We also noted an absence of co-localization between HELLP(214-271) and HET-s or
284 HELLP(214-271) and HELLF(209-277) prion forms (Fig. 4, Table S8).

285

286 ## *P. anserina* and *C. globosum* [π] prions cross-seed and co-localize

287 It was shown previously that HET-S PFDs homologs from *P. anserina* and *Fusarium*
288 *graminearum* which share about 41% identity do cross-seed (29). We wondered whether the
289 36% similarity between the PP-regions of HELLP and CgHELLP would also allow for cross-
290 seeding (as suggested by the fact that pairwise similarities between the different PP-motifs
291 within the *C. globosum* PP-gene cluster or within the *P. anserina* PP-gene pair are in the range
292 of 32-48%, Fig. 1B).

293 Upon confrontation, [π] GFP-HELLP(214-271) donor strains invariably converted GFP-
294 CgHELLP(215-278) [π*] recipient strains and conversely [π] CgHELLP(215-278) strains
295 converted GFP-HELLP(214-271) [π*] recipients (Table S5). We analyze the cross-induction of
296 cell death activity of the full-length CgHELLP and HELLP proteins in barrage tests (Fig. 5B and
297 Tables S5, S6). GFP-CgHELLP(215-278) [π] strains produced a barrage reaction to strains
298 expressing HELLP and conversely GFP-HELLP(214-271) [π] produced a barrage reaction to
299 strains expressing CgHELLP. However, this was only true when HELLP was highly expressed as
300 a transgene. No barrage was observed in confrontation to wild type. This result suggest that
301 heterologous activation of HELLP by GFP-CgHELLP(215-278) is less efficient than homotypic
302 activation by GFP-HELLP(214-271).

303 To examine if the two PFD regions could co-localize *in vivo*, strains co-expressing
304 HELLP(214-271)-RFP and GFP-CgHELLP(215-278) were obtained and analyzed by fluorescence
305 microscopy (Fig. 5A, Tables S7 and 8). We initially observed diffuse fluorescence
306 corresponding to the [π*] state and after a few days, foci appeared concomitantly for the two
307 proteins. There was no co-existence of diffuse and foci forms suggesting cross-conversion of
308 HELLP and CgHELLP (Table S7). Moreover, we observed a significant co-localization indicating

309 co-aggregation of the two prions (Fig. 5A).

310 We conclude that, as previously reported for *F. graminearum* and *P. anserina* [Het-s], the
311 "species-barrier" for prion seeding can be crossed for these PP-motifs. This result is consistent
312 with the fact that the level of within-cluster similarity of the PP-motifs is comparable to the
313 similarity between CgHELLP and HELLP PP-motifs. Nevertheless, the absence of barrage
314 reaction between strains expressing $[\pi]^{Cg}$ prions and HELLP at wild-type level suggests that
315 homotypic or within-cluster interactions are more efficient to activate the cell-death activity
316 of the full-length protein.

317

318 **The RHIM motifs of human RIP1 and RIP3 kinases form prions in *P. anserina***

319 The PP-motif as found in HELLP shows sequence homology to the mammalian RHIM
320 amyloid motif (Fig. 1B). We thus envisioned that akin to the PP-motif, mammalian RHIMs
321 might behave as PFDs when expressed in Podospora. We expressed the RIP1(524-551) and
322 RIP3(444-469) regions fused to GFP or RFP in *Δhellp Δhet-s Δhellf* strains (Fig. 6). Initially
323 fluorescence was diffuse and cytoplasmic and foci appeared spontaneously after a few days
324 of growth. The rate of spontaneous transition to the aggregated state was monitored as
325 previously for HELLP (Table 1). For RIP3(444-469), the rates were comparable to the PP-motif
326 with the highest rate observed with GFP in N-terminal position. For RIP1 RHIM, spontaneous
327 rate of foci formation was lower especially for the two GFP fusions. The induced conversion
328 through cytoplasmic infection (with the corresponding foci form) was equally effective for the
329 RIP1 and RIP3 RHIM-motifs (Table 1). We designated the diffuse and infectious foci states
330 [Rhim*] and [Rhim] respectively.

331 Strains expressing RIP1(524-551) foci induced formation of RIP3(444-469) foci and the
332 converse was true (Fig. 7) showing cross-conversions between $[Rhim]^{RIP1}$ and $[Rhim]^{RIP3}$ prions.

333 In these assays, heterotypic cross-induction rates between [Rhim]^{RIP1} and [Rhim]^{RIP3} were not
334 significantly different from homotypic induction rates. To further analyze the interaction of
335 [Rhim] prions propagated in *P. anserina*, we co-expressed RIP1(524-551) and RIP3(444-469)
336 fused to GFP or RFP in the same strain (Fig. 8, Tables S7 and S8). Strains co-expressing
337 RIP3(444-469) fused with GFP and RFP, or RIP1(524-551) fused with GFP and RFP were used
338 as positive control (Fig. 8B) and showed co-localization with overlapping foci. In RIP1(524-551)
339 and RIP3(444-469) co-expression, diffuse fluorescence was observed initially. Then, foci
340 formed concomitantly for both proteins. We observed no situation in which one of the protein
341 formed foci while the other remained diffuse as previously observed for heterotypic PP-motif
342 interactions (Fig. 8, Table S8). RIP1(524-551) and RIP3(444-469) foci co-localized in the cell
343 (Fig. 8, Table S8), often in the close vicinity of the septa where they appeared as aligned dots.
344 We conclude that, the RHIM containing RIP3(444-469) and RIP1(524-551) regions of 26
345 and 28 amino acids in length behave as PFDs *in vivo* in *P. anserina* and lead to the expression
346 of two alternate phenotypes we termed [Rhim*] and [Rhim]. In addition, the RIP1 and RIP3
347 [Rhim] prions efficiently cross-seed and co-localize consistent with the fact that in mammalian
348 cells and *in vitro*, RIP1 and RIP3 interact through their RHIM regions to form amyloid
349 heteropolymers (25).
350

351 **The [Rhim] and [π] prions partially cross-seed**

352 Based on the similarity of PP and RHIM motifs and on the fact that RIP1 and RIP3 RHIM
353 motifs propagate as prions *in vivo* in Podospora, it was conceivable that [π] and [Rhim] prions
354 might cross seed to some extent. To examine possible interaction between [Rhim] and [π]
355 prions, HELLP(214-271)-RFP [π*], GFP-RIP3(444-496) and GFP-RIP1(524-551) [Rhim*] strains

356 were confronted with [π] and [Rhim] strains (Fig. 7). After four days, the recipient strains were
357 sampled, subcultured, and analyzed for the presence of foci by fluorescence microscopy. We
358 deliberately chose transformants expressing moderate levels of the fusion proteins to
359 decrease the rates of spontaneous prion formation in these experiments. In these test
360 conditions, spontaneous prion formation was in the range of 10 to 20% for all constructs.
361 Homotypic interactions led to 80 to 90% prion conversion (as mentioned above, high
362 conversion rates were observed for heterotypic conversion of GFP-RIP3(444-496) [Rhim*] by
363 GFP-RIP1(524-551) [Rhim] and GFP-RIP1(524-551) [Rhim*] by GFP-RIP3(444-496) [Rhim]). [π]
364 prions induced formation of both [Rhim] prions at a rate of about 60%. Conversely, both
365 [Rhim] prions induced formation of [π] prions at a similar rate (Fig. 7). These results show cross
366 conversion between [Rhim] and [π] prions. The conversion is however less efficient as in the
367 case of homotypic or intra-kingdom $[Rhim]^{RIP1}$/$[Rhim]^{RIP3}$ or $[\pi]^{Pa}$/$[\pi]^{Cg}$ interactions.

368 We also tested the ability of the two [Rhim] prions to induce the conversion of [Het-
369 s*] strains to the [Het-s] phenotype and observed cross-induction (18 transformants for each
370 [Rhim] prion tested in triplicate). This result is in line with the previous results on the absence
371 of cross-interaction between [π] and the other amyloid signaling pathways of *P. anserina* and
372 are thus rather expected.

373 To explore interactions between [π] and [Rhim] further, HELLP and RIP3 (or RIP1) PFDs
374 fused to GFP or RFP were co-expressed in the same strain and transformants were analyzed
375 by fluorescence microscopy (Fig. 9, S6, Tables S7, S8). Consistent with the conversion
376 experiments indicating partial cross-seeding, we could observe cells where one of the protein
377 formed foci while the other remain in the diffused state as observed previously for non-cross
378 seeding prions (Fig. 9 and S6, Table S7). In [π]/[Rhim] cells, the fraction of the foci that co-
379 localized was higher (~68 %) than between non-cross seeding prions (such as HET-s and HELLP

380 for instance, ~5 %) but lower than in homotypic or [Rhim]^{RIP1}/[Rhim]^{RIP3} or [π]^{Pa}/[π]^{Cg} prions
381 (~82-96%). In addition, even in mixed foci the co-localization is imperfect with RFP and GFP
382 fluorescence that only partially overlapped (Fig. 9). This phenomenon of patchy co-localization
383 has already been observed during coexpression of the HET-s proteins of *F. graminearum* and
384 *P. anserina* (29). The same [π]/[Rhim] interaction experiments were also carried out with
385 CgHELLP(215-278) and similar results were obtained (Fig. S7, Tables S7 and S8). [π]^{Cg} and
386 [Rhim] prions were found to partially cross-seed. And in this case also, there was a partial co-
387 localization of [Rhim] and [π] prions, a situation that is distinct both from the total lack of
388 interaction seen between [π] and [Het-s] and [Φ] prions and from the strong interactions seen
389 between RIP1 and RIP3 [Rhim] prions on one hand and HELLP and CgHELLP [π] prions on the
390 other hand.
391
392 The above [Rhim]/[π] cross-seeding and co-localization experiments suggest that RHIM
393 and PP-motifs can interact but that this interaction is less efficient than PP-homotypic
394 interactions. We wondered whether [Rhim] prions could nonetheless induce at least partially,
395 HELLP or CgHELLP toxicity in a setting favoring [Rhim]/HELLP interactions. We thus co-
396 expressed in the same strain GFP-RIP3(444-469) or GFP-RIP1(524-551) and HELLP-RFP or
397 CgHELLP to determine whether prion conversion of [Rhim] in this strain would lead to growth
398 alterations (self-incompatibility). Positive controls corresponding to cross-interacting
399 incompatible combinations ([π]/HELLP) or negative controls corresponding non-interacting
400 combinations ([ϕ] or [Het-s]/HELLP or [Rhim]/HET-S) were used for comparison (Table 2). In
401 each combination, growth of a population of 12 to 39 transformants was observed before or
402 after infection with the respective prion. Before prion infection, growth was normal for the
403 vast majority of the transformants. After prion infection, a large fraction of the transformants

404 (about 80%) co-expressing RHIM constructs and full length HELLP or CgHELLP showed growth
405 defects (Table 2 and Fig. 10). A similar proportion of growth defects was observed in known
406 cross-interacting combinations while growth alterations where not significantly increased in
407 non-interacting combinations. The growth alteration phenotypes were highly heterogeneous
408 (Table2, Fig. 10) ranging from sublethal growth to minor growth alteration. This phenotypic
409 heterogeneity is typical of such self-incompatible situations and was also observed for the
410 control self-incompatible strains. This heterogeneity is thought to result from differences in
411 transgene copy number and integration site in the different transformants and "escape" from
412 self-incompatibility that is strongly selected for and often manifests as sector formation that
413 recover close to normal growth and can occur by transgene mutation or deletion and in this
414 particular case from prion curing. Strains with [Rhim] prions do not lead to a barrage reaction
415 when confronted to strains expressing full length HELLP suggesting that the RHIM/HELLP
416 interaction is not efficient enough to induce a massive cell-death reaction and barrage
417 formation. We however observed cell death in fusion cells between strains expressing HELLP-
418 RFP and GFP-RIP3(444-469) or GFP-RIP1(524-551) [Rhim] strains (Fig. S9). These results are
419 consistent with the conversion experiments and indicate that [Rhim] prions are able to induce
420 to some extent toxicity of HELLP (and CgHELLP) albeit at a lower efficiency than [π] prions.
421

422 # Discussion

423 A number of innate immune pathways function following a principle of "signaling by
424 cooperative assembly formation" (SCAF) (30). Upon recognition of PAMPs (Pathogen-
425 associated molecular pattern) or MAMPs (Microbe-associated molecular pattern), receptors
426 assemble into higher-order complexes or "supramolecular organizing centers" (SMOCs) (31).

427 Following ligand recognition, the sensor modules oligomerize and recruit adaptor or effector
428 proteins -often via homotypic interactions- that further amplify the oligomerization process
429 and form cooperative, open-ended polymers (typically filaments). This general scheme applies
430 to many immune signaling modules including the RIG-I-like receptors, the AIM2-like receptors
431 and to NLRs. Formation of higher-order assemblies entitles such signaling cascade with signal
432 amplification, sharp threshold behavior and noise reduction. In fact, this so-called prion-like
433 polymerization process can involve nucleation of either folded globular domains such as the
434 TIR or Death domains (32, 33) or short amyloid motifs. The first such motif is RHIM identified
435 in the necroptosis pathway in mammals and allows for assembly of the necrosome formed by
436 the RIP1 and RIP3 kinases (23). RHIM-like motif also regulate amyloid formation in innate
437 immune cascades in Drosophila (24). In addition, several NLR-associated amyloid signaling
438 motifs were identified in filamentous fungi and more recently in multicellular bacteria (18, 34).
439 Among them is the PP-motif that shows similarity to the animal RHIM and RHIM-like motifs
440 (22). We identify here in the species *Podospora anserina*, a PP-motif two-component system
441 comprising a NLR termed PNT1 and a cell-death execution protein termed HELLP. As
442 previously reported for CgHELLP from *C. globosum*, the N-terminal HELL domain of HELLP
443 shows homology to the 4HB domain of MLKL responsible for membrane permeation in
444 mammalian necroptosis. HELLP induced PCD thus appears to be related to a family of
445 evolutionary widespread form of immune PCD which encompasses fungal cell death,
446 necroptosis and cell death associated with the hypersensitive response in plants (22, 35, 36).
447 We propose that PNT1 and HELLP constitute a third amyloid immune-related signaling cascade
448 controlling cell fate in *P. anserina*. We show the absence of cross-induction between the three
449 *P. anserina* systems allowing for the co-existence of three independent amyloid signaling
450 cascades in the same species. It is believed that fungal NLRs akin to their plant and animal

451 counterparts represent innate immune receptors that regulate response to pathogen and
452 symbiotic interactions in fungi. The three amyloid-associated NLRs identified in Podospora
453 share the fact that their WD or TPR repeat ligand binding domain is highly polymorphic in
454 natural populations consistent with the proposed role as immune receptor (13, 14). Yet,
455 except in the specific case of NLRs involved in incompatibility systems the nature of the ligands
456 activating these NLRs are currently unknown. Compared to the two other systems, the
457 NWD2/HET-S is characterized by the fact that this system has been exaptated as an
458 allorecognition system in [Het-s]/HET-S incompatibility (37). It has been possible
459 experimentally, to derive incompatibility systems analogous to [Het-s]/HET-S from both HELLP
460 and HELLF. It will be of interest in the future to survey, natural Podospora strains to determine
461 whether exaptation of allorecognition incompatibility might have also occurred from HELLP
462 and HELLF. It is also of note, that the *Chaetomium globosum* and *Podospora anserina* PP-based
463 signalosome differ in the sense that the *Chaetomium* system has three components and
464 involves also CgSBP, a lipase also comprising a PP-motif and that is targeted to the membrane
465 region by CgHELLP. The present study is superior to the previous study on the PP-gene cluster
466 in the sense that HELLP function is being studied here in the native context rather than by
467 heterologous expression (22).

468 So far, four mammalian proteins involved in necroptosis and five drosophila proteins also
469 involved in immune signaling rely on RHIM-based amyloid signaling (23, 24). The fact that a
470 range of viruses express RHIM containing proteins and that pathogenic bacteria express an
471 enzyme that specifically cleave host RHIMs to prevent necrosome assembly highlight the
472 crucial role of RHIM-based interactions in the host innate immune response against microbial
473 infection (38). PP-motifs of CgHELLP and HELLP resemble RHIM motifs (Fig. 1B). This similarity
474 is centered in the G-ϕ-Q-ϕ-G core of the motif. Mompeán and co-workers resolved the

475 structure of human RIP1-RIP3 amyloid region as a serpentine fold with turns and kinks
476 resulting in an enclosed oblong-shaped hydrophobic core stabilized by N and Q ladders and Y
477 stacking (25). RHIM-related motif appear to represents a new class of amyloid fold distinct
478 from the HRAM β-solenoid fold of HET-s but nonetheless presenting common features with
479 them as with other amyloid forming domains such as conservation of G/N/Q residues. N and
480 Q allow for formation of H-bonded N/Q ladders and G connect short adjacent β-strands (11,
481 39–41). The fungal PP-motifs show strong conservation of the pseudopalindromic structure
482 centered on the Q residue along with conservation of flanking N and G residues. We find here
483 that the RHIM motifs of RIP1 and RIP3 behave as PFDs when expressed in Podospora and thus
484 behave analogously to PP-motifs in that respect. The simple *in vivo* Podospora model might
485 represent a useful tool to study RHIM motif assembly and interaction for instance to screen
486 for inducers or inhibitors of RIP1/RIP3 interactions.

487 Importantly, we find that [Rhim] and [π] prions cross-seed, albeit not as efficiently as
488 RHIM motifs or fungal PP-motifs. These results suggest both a structural similarity between
489 RHIM and PP-amyloids and substantial differences since the efficiency of prion seeding is
490 clearly distinct from that of homotypic or intraspecific seeding. Extensive structural analyses
491 of the amyloid fibers of HELLP or CgHELLP will be required to determine to which extend PP-
492 based amyloid polymers share the same fold as RIP1-RIP3. It appears however that the partial
493 cross-seeding between PP and RHIM support a model of a common evolutionary origin of the
494 two motifs. In this context, it is interesting to note that in addition to the RHIM-like motifs
495 described in Drosophila a RHIM-related amyloid motif termed BASS3 was also identified in
496 multicellular bacteria (34). It might be that the RHIM-related motif represent an archetypal
497 amyloid motif largely shared through evolution while other motifs such as HRAMs or other
498 bacterial signaling motifs have a more restricted phylogenetic distribution.

499

500 # Materials and Methods

501 ## Gene annotation

502 The Pa_5_8070 and Pa_5_8060 genes were annotated manually using two intron prediction
503 softwares, the GENSCAN Web server at MIT (genes.mit.edu/GENSCAN.html) and the
504 NetGene2 Web server (www.cbs.dtu.dk/services/NetGene2/), and using blastn searches
505 against EST sequences at ncbi and RNASEQ data from (42). A single 47pb intron was identified
506 in nucleotide position 429 to 475 of the Pa_5_8070 ORF, this newly defined ORF encodes a
507 271 aa protein named HELLP. A single intron of 54 pb was identified in nucleotide position 95
508 to 148 of the ORF of Pa_5_8060, TPR repeat number in the 3' part of the ORF is variable in *P.*
509 *anserina* strains, we described here the ORF of the S Orsay reference strain encoding a 971 aa
510 protein named PNT1.

511

512 ## Strains and plasmids

513 The *P. anserina* strains used in this study were wild-type *het-s* or *het-S* and the strains *Δhellp*
514 (*ΔPa_5_8070*) *het-s°* (22) and *Δhellp (ΔPa_5_8070) Δhet-s (ΔPa_3_620) Δhellf (ΔPa_3_9900)*
515 obtained by crossing the *Δhet-s Δhellf* strain (20) with the *Δhellp het-s°* strain. The *Δhellp het-*
516 *s°* strain was used as recipient strain for the expression of molecular fusions of full length
517 HELLP or PP motif-containing regions of HELLP and the GFP (green fluorescent protein) or RFP
518 (red fluorescent protein). These fusions were expressed from plasmids based on the pGEM-T
519 backbone (Promega) named pOP plasmids (22), containing either the GFP or RFP, or in a
520 derivative of the pAN52.1 GFP vector (27), named pGB6-GFP plasmid. In both cases, the
521 molecular fusions were under the control of the strong constitutive *P. anserina* gpd

522 (glyceraldehyde-3-phosphate dehydrogenase) promoter. The *Δhellp het-s°* strain was
523 transformed as described (43) with a fusion construct along with a second vector carrying a
524 phleomycin-resistance gene ble, pPaBle (using a 10:1 molar ratio). Phleomycin-resistant
525 transformants were selected, grown for 30 h at 26°C and screened for the expression of the
526 transgenes using fluorescence microscopy. The *hellp* gene and the *hellp(171-271)* and
527 *hellp(214-271)* gene fragments were amplified with the respective 5' forward oligonucleotides
528 5' ggcttaattaaATGGATCCTCTCAGTATCACAGC 3', 5'
529 ggcttaattaaATGATCACAGCGACAAACGATCAG 3' and 5'
530 ggcttaattaaATGAAAGTACTGCATGAATCGCGC 3' and a same 3' reverse oligonucleotide 5'
531 ggcagatcttgctccCCCCCTTCGGCCAAATGTAG 3' (capital letters correspond to *P. anserina*
532 genomic DNA sequences). The PCR products were cloned upstream of the GFP or RFP coding
533 sequence in the pOP plasmids using *Pac*I/*Bgl*II restriction enzymes to generate the pOPhellp-
534 GFP, pOPhellp-RFP, pOPhellp(171-271)-GFP, pOPhellp(171-271)-RFP, pOPhellp(214-271)-GFP
535 and pOPhellp(214-271)-RFP vectors in which in addition to the *Bgl*II site, a two amino acid
536 linker (GA) was introduced between the sequences encoding HELLP and GFP or RFP. *hellp(171-*
537 *271)* and *hellp(214-271)* were also amplified with the respective 5' forward oligonucleotides
538 5' ggcgcgcggccgcATCACAGCGACAAACGATCAG 3', 5'
539 ggcgcgcggccgcATCACAGCGACAAACGATCAG 3' and the same 3' reverse oligonucleotide 5'
540 ggcggatccCTACCCCCTTCGGCCAAATG 3' and cloned downstream of the GFP using *Not*I/*Bam*HI
541 restriction enzymes to generate the plasmids pGB6-GFP-hellp(171-271) and pGB6-GFP-
542 hellp(214-271).

543 To investigate the co-localization of HELLP with CgHELLP or of HELLP with HELLF or HET-s,
544 the *Δhellp Δhet-s Δhellf* strain was transformed both with vectors expressing fluorescently
545 tagged versions of full-length or truncated HELLP described above and with fluorescently

546 tagged versions of full-length or truncated HELLF, HET-s, HET-S or CgHELLP previously
547 described (20, 22, 27): pOPhellf-GFP, pOPhellf(209-277)-RFP, pOPhellf(209-277)-GFP,
548 pOPhellf(L52K)-GFP, pOPhet-s-RFP, pGPD-het-S-GFP, pOPhet-S-RFP, pGB6-GFP-Cghellp(215-
549 278).

550 In the same way the sequence encoding the first 31 amino acids of *pnt1 (Pa_5_8060)* was
551 amplified with oligonucleotides 5' ggcttaattaaATGTCAGACAGTTATCGTTTCGGC 3' and 5'
552 ggcagatcttgctccTGGCGCCTGCAGGAAAGTATTG 3' and cloned in the pOP plasmids using
553 *Pac*I/*Bgl*II restriction enzymes to generate the pOPpnt1(1-31)-GFP and the pOPpnt1(1-31)-
554 RFP. The *Δhellp Δhet-s Δhellf* strain was transformed with these vectors (and pPaBle) either
555 alone or with pOPhellp(214-271)-RFP or pGB6-GFP-hellp(214-271).

556 For heterologous expression in *E. coli*, we cloned *hellp(214-271)* in pET24 (Novagen) using
557 the *Nde*I/*Xho*I restrictions sites. The gene fragment *hellp(214-271)* was amplified with
558 oligonucleotides 5' agccatatgAAAGTACTGCATGAATCGCGC 3' and 5'
559 agcctcgagCCCCCTTCGGCCAAATGTAG 3' and cloned in front of a polyhistidine-tag to generate
560 pET24-hellp(214-271)-6xhis plasmid.

561 For the expression of RIP3(444-469) and RIP1(524-551), PCR products were amplified with
562 5' ggcttaattaaATGGTTACCGGTCGTCCGCTG 3' and 5'
563 ggcagatcttgctccCTGCATGGTCAGGTAGTTGTTG 3' or 5' ggcgcggccgcGTTACCGGTCGTCCGCTGG
564 3' and 5' ggcGGATCCTTACTGCATGGTCAGGTAGTTG 3' for RIP3 and with 5'
565 ggcttaattaaATGACTGACGAATCCATCAAATACACC 3' and 5'
566 ggcagatcttgctccGCCGCCGATTTCCATGTAGTT 3' or 5'
567 ggcgcggccgcACTGACGAATCCATCAAATACACC 3' and 5'
568 ggcGGATCCTTAGCCGCCGATTTCCATGTAGTT 3' for RIP1 and cloned as described above in the

569 pOP plasmids using *Pac*I/*Bgl*II restriction enzymes, or in pGB6-GFP plasmid using *Not*I/*Bam*HI
570 restriction enzymes.
571

572 **Microscopy**

573 *P. anserina* hyphae were inoculated on solid medium and cultivated for 24 to 72 h at 26°C.
574 The medium was then cut out, placed on a glass slide and examined with a Leica DMRXA
575 microscope equipped with a Micromax CCD (Princeton Instruments) controlled by the
576 Metamorph 5.06 software (Roper Scientific). The microscope was fitted with a Leica PL APO
577 100X immersion lens. To observe cell-death reactions and HELLP re-localization, HELLP-GFP or
578 HELLP-RFP expressing strains were inoculated at a distance of 2 cm from a strain expressing
579 one of the fusion protein containing either a HELLP PFD or PNT1(1-31), RIP3(444-469) or
580 RIP1(524-551) fused to GFP or RFP. The confrontation zone between the two strains was
581 observed 12 to 48 hours after contact. For methylene blue staining an aqueous 0.5% solution
582 was put directly on the mycelium for 1 min followed by washing with distilled water before
583 observation as described above.
584 For HELLP fibrils observations, negative staining was performed: aggregated proteins were
585 adsorbed onto Formvar-coated copper grids (400 mesh) and allowed to dry for 15 min in air,
586 grids were then negatively stained 1 min with 10 µL of freshly prepared 2% uranyl acetate in
587 water, dried with filter paper, and examined with a Hitachi H7650 transmission electron
588 microscope (Hitachi, Krefeld, Germany) at an accelerating voltage of 120 kV. TEM was
589 performed at the Pôle Imagerie Électronique of the Bordeaux Imaging Center using a Gatan
590 USC1000 2k x 2k camera.
591

592 **Incompatibility assays (barrage tests).**

593 Methods for determination of incompatibility phenotypes were previously described (20, 44).
594 In brief, incompatibility phenotypes were determined by confronting strains on solid corn-
595 meal agar medium and a 'barrage' reaction (abnormal contact lines forming upon
596 confrontation of incompatible strains) was assessed 3 days post-contact. The [π] phenotype
597 (acquisition of the [π] prion) was assessed as the ability of a strain to form a barrage with a
598 wild-type strain or with a *Δhellp* bearing a transgene encoding full-length HELLP in fusion with
599 GFP or RFP, named tester strain. Cross reaction between the different prion systems was also
600 assessed in barrage tests as the ability of a prion containing strain (either [π], [Rhim], [Het-s]
601 or [Φ]) to form a barrage with a strain expressing one of the full length HeLo or HELL containing
602 proteins HELLP, CgHELLP, HELLF or HET-S. In these experiments strains previously described
603 by Daskalov and colleagues were used (20, 22).

604

605 **Prion propagation**

606 Methods for determination of prion formation and propagation were previously described (20,
607 44). Prion formation and propagation can be observed either using microscopy by monitoring
608 the apparition of dots or using barrage tests by observing the formation of a barrage with the
609 tester strain.

610 Spontaneous prion formation is first monitored as the rate of spontaneous acquired prion
611 phenotype (dots) in the initially prion-free subculture after 5, 11 and 19 days of growth at 26°C
612 on corn-meal agar using microscopy as described. Then transformants were re-observed at
613 least 60 days after transformation to confirm prion acquisition. For [π] strains, barrage tests

614 were realized 5, 19 and after at least 60 days and a strict correlation between presence of dots
615 and barrage formation with HELLP expressing strains was always observed.
616 Prion formation can also be measured as the ability to propagate prions from a donor strain
617 (containing prion) to a prion-free strain (induced strain). In practice, prion-free strains are
618 confronted on solid corn-meal agar medium for 4 to 6 days (this step is mentioned as previous
619 contact with in Tables) before being subcultured and observed by fluorescence microscopy
620 and analyzed in barrage tests. As indicated in figure legends, at least 12 different
621 transformants were used and the tests were realized in triplicates. Again for [π] strains,
622 barrage and dots presence are strictly correlated. Prion acquisition through induction can also
623 be visualized directly on solid medium by positioning the inocula of donor and prion-free
624 strains closer than the tester strain (see Fig. S2) to allow prion propagation before contact
625 with the tester strain.
626 It is to note that transformants were randomly tested for prion formation allowing
627 various expression levels of the transgene (high levels of expression are usually associated
628 with very rapid spontaneous prion formation) except for the cross conversion test (see Fig. 8
629 and S8) where transformants expressing moderate level of transgene were preferred to limit
630 the rate of spontaneous transition within the timing of the experiment that could mask the
631 prion induction. For this experiment, a statistical analysis was performed using two tails
632 Fisher's test to determine p-values and validate test result as indicated in the figure legend.
633

634 **Protein preparation and fibril formation**

635 HELLP(214-271) protein was expressed in *E. coli* BL21-CodonPlus®-RP competent cells as
636 insoluble proteins and purified under denaturing conditions using its terminal 6 histidine tag
637 as previously described (45). Briefly, cells were grown at 37°C in DYT medium to 0.6 OD_{600} and

638 expression was induced with 1 mM isopropyl β-D-1-thiogalactopyranoside. After, 4 h, cells
639 were harvested by centrifugation, frozen at -80°C sonicated on ice in a lysis buffer (Tris 50
640 mM, 150 mM NaCl, pH 8) and centrifuged for 20 min at 20,000 g to remove *E. coli*
641 contaminants. The pellet containing HELLP(214-271) in inclusion bodies was washed in the
642 same buffer and resuspended in denaturing buffer (8M guanidinium HCl, 150 mM NaCl, and
643 100 mM Tris-HCl, pH 8) until complete solubilization. The lysate was incubated with Talon
644 Resin (CLONTECH) for 1 h at 20°C, and the resin was extensively washed with 8 M urea, 150
645 mM NaCl, and 100 mM Tris-HCl, pH 8. The protein was eluted from the resin in the same buffer
646 containing 200 mM imidazole. The protein HELLP(214-271) was pure as judged by sodium-
647 dodecyl-sulfate polyacrylamide-gel electrophoreses (SDS-PAGE) followed by Coomassie-Blue
648 staining and yield was in the range of ~2-4 mg of protein per liter of culture. To eliminate urea,
649 elution buffer was replaced by overnight dialysis at 4°C against Milli-Q water. Fibrils formation
650 resulted spontaneously from dialysis process followed by sample storage at 4°C for 7 days.
651 Other conditions were used for sample preparation to test the influence of salt or acidic buffer
652 on the fibrils formation: presence or absence of 500 mM NaCl in the dialysis buffer,
653 replacement of dialysis by 50 times dilution in Milli-Q water or in ammonium acetate buffer
654 100 mM pH 4.5, they all resulted in spontaneous appearance of fibrils.
655

656 **Bioinformatics methods**

657 Blast analyses on the *P. anserina* genome were achieved on the *Podospora anserina* Genome
658 Project site (podospora.i2bc.paris-saclay.fr/). Sequence alignments were performed with
659 Clustal Omega or MAFFT at (www.ebi.ac.uk) and edited with Jalview (www.jalview.org/). To
660 generate the HMM profile signatures for PP and RHIM, psi-blast searches were performed at
661 (blast.ncbi.nlm.nih.gov) using the HELLP PP sequence and the RHIM motif of human RIP3 and

matching sequences were aligned with Clustal Omega and the alignment was analyzed with Skylign (skylign.org). Secondary structure predictions were performed with PSIPRED (bioinf.cs.ucl.ac.uk/psipred/). Hidden Markov Model searches were performed using HHPred (toolkit.tuebingen.mpg.de) and Jackhhmer (www.ebi.ac.uk/Tools/hmmer/search/phmmer), both with default settings. The prediction of transmembrane helix was performed with the TMHMM server (www.cbs.dtu.dk/services/TMHMM).

Author Contributions

Conceptualization: Thierry Bardin, Asen Daskalov, Sven J. Saupe, Virginie Coustou

Data curation: Thierry Bardin, Asen Daskalov, Sophie Barrouilhet, Sven J. Saupe, Virginie Coustou

Formal analysis: Thierry Bardin, Asen Daskalov, Sophie Barrouilhet, Sven J. Saupe, Virginie Coustou

Funding acquisition: Sven J. Saupe

Investigation: Thierry Bardin, Asen Daskalov, Sophie Barrouilhet, Alexandra Granger-Farbos, Bénédicte Salin, Corinne Blancard, Virginie Coustou

Methodology: Thierry Bardin, Asen Daskalov, Alexandra Granger-Farbos, Bénédicte Salin, Corinne Blancard, Sven J. Saupe, Virginie Coustou

Project administration: Sven J. Saupe, Virginie Coustou

Resources: Alexandra Granger-Farbos, Bénédicte Salin, Corinne Blancard, Sven J. Saupe, Virginie Coustou

Supervision: Sven J. Saupe, Virginie Coustou

Validation: Thierry Bardin, Asen Daskalov, Sven J. Saupe, Virginie Coustou

Visualization: Thierry Bardin, Asen Daskalov, Sven J. Saupe, Virginie Coustou

Writing: Sven J. Saupe, Virginie Coustou

688 # References

689 1. Prusiner S. 1982. Novel proteinaceous infectious particles cause scrapie. Science 216:136.

690 2. Colby DW, Prusiner SB. 2011. Prions. Cold Spring Harbor Perspectives in Biology 3:a006833–
691 a006833.

692 3. Wickner RB, Edskes HK, Son M, Bezsonov EE, DeWilde M, Ducatez M. 2018. Yeast Prions
693 Compared to Functional Prions and Amyloids. Journal of Molecular Biology 430:3707–3719.

694 4. Coustou V, Deleu C, Saupe S, Begueret J. 1997. The protein product of the het-s heterokaryon
695 incompatibility gene of the fungus Podospora anserina behaves as a prion analog. Proc Natl Acad
696 Sci U S A 94:9773–9778.

697 5. Saupe SJ. 2011. The [Het-s] prion of Podospora anserina and its role in heterokaryon
698 incompatibility. Semin Cell Dev Biol 22:460–468.

699 6. Balguerie A, Dos Reis S, Ritter C, Chaignepain S, Coulary-Salin B, Forge V, Bathany K, Lascu I,
700 Schmitter J-M, Riek R, Saupe SJ. 2003. Domain organization and structure-function relationship
701 of the HET-s prion protein of Podospora anserina. EMBO J 22:2071–2081.

702 7. Seuring C, Greenwald J, Wasmer C, Wepf R, Saupe SJ, Meier BH, Riek R. 2012. The mechanism of
703 toxicity in HET-S/HET-s prion incompatibility. PLoS Biol 10:e1001451.

704 8. Nazabal A, Dos Reis S, Bonneu M, Saupe SJ, Schmitter J-M. 2003. Conformational transition
705 occurring upon amyloid aggregation of the HET-s prion protein of Podospora anserina analyzed
706 by hydrogen/deuterium exchange and mass spectrometry. Biochemistry 42:8852–8861.

707 9. Ritter C, Maddelein M-L, Siemer AB, Lührs T, Ernst M, Meier BH, Saupe SJ, Riek R. 2005.
708 Correlation of structural elements and infectivity of the HET-s prion. Nature 435:844–848.

709 10. Sen A, Baxa U, Simon MN, Wall JS, Sabate R, Saupe SJ, Steven AC. 2007. Mass analysis by scanning
710 transmission electron microscopy and electron diffraction validate predictions of stacked beta-
711 solenoid model of HET-s prion fibrils. J Biol Chem 282:5545–5550.

712 11. Wasmer C, Lange A, Van Melckebeke H, Siemer AB, Riek R, Meier BH. 2008. Amyloid fibrils of the
713 HET-s(218-289) prion form a beta solenoid with a triangular hydrophobic core. Science
714 319:1523–1526.

715 12. Mathur V, Seuring C, Riek R, Saupe SJ, Liebman SW. 2012. Localization of HET-S to the cell
716 periphery, not to [Het-s] aggregates, is associated with [Het-s]-HET-S toxicity. Mol Cell Biol
717 32:139–153.

718 13. Daskalov A, Habenstein B, Martinez D, Debets AJM, Sabaté R, Loquet A, Saupe SJ. 2015. Signal
719 transduction by a fungal NOD-like receptor based on propagation of a prion amyloid fold. PLoS
720 Biol 13:e1002059.

721 14. Dyrka W, Lamacchia M, Durrens P, Kobe B, Daskalov A, Paoletti M, Sherman DJ, Saupe SJ. 2014.
722 Diversity and variability of NOD-like receptors in fungi. Genome Biol Evol 6:3137–3158.

723 15. Jones JDG, Vance RE, Dangl JL. 2016. Intracellular innate immune surveillance devices in plants
724 and animals. Science 354.

725 16. Daskalov A, Paoletti M, Ness F, Saupe SJ. 2012. Genomic clustering and homology between HET-
726 S and the NWD2 STAND protein in various fungal genomes. PLoS ONE 7:e34854.

727 17. Cai X, Chen J, Xu H, Liu S, Jiang Q-X, Halfmann R, Chen ZJ. 2014. Prion-like polymerization
728 underlies signal transduction in antiviral immune defense and inflammasome activation. Cell
729 156:1207–1222.

730 18. Loquet A, Saupe SJ. 2017. Diversity of Amyloid Motifs in NLR Signaling in Fungi. Biomolecules 7.

731 19. Daskalov A, Dyrka W, Saupe SJ. 2015. Theme and variations: evolutionary diversification of the
732 HET-s functional amyloid motif. Sci Rep 5:12494.

733 20. Daskalov A, Martinez D, Coustou V, El Mammeri N, Berbon M, Andreas LB, Bardiaux B, Stanek J,
734 Noubhani A, Kauffmann B, Wall JS, Pintacuda G, Saupe SJ, Habenstein B, Loquet A. 2020.
735 Structural and molecular basis of cross-seeding barriers in amyloids. bioRxiv 2020.07.06.188508.

736 21. Murphy JM, Czabotar PE, Hildebrand JM, Lucet IS, Zhang J-G, Alvarez-Diaz S, Lewis R, Lalaoui N,
737 Metcalf D, Webb AI, Young SN, Varghese LN, Tannahill GM, Hatchell EC, Majewski IJ, Okamoto T,
738 Dobson RCJ, Hilton DJ, Babon JJ, Nicola NA, Strasser A, Silke J, Alexander WS. 2013. The
739 Pseudokinase MLKL Mediates Necroptosis via a Molecular Switch Mechanism. Immunity 39:443–
740 453.

741 22. Daskalov A, Habenstein B, Sabaté R, Berbon M, Martinez D, Chaignepain S, Coulary-Salin B,
742 Hofmann K, Loquet A, Saupe SJ. 2016. Identification of a novel cell death-inducing domain reveals
743 that fungal amyloid-controlled programmed cell death is related to necroptosis. Proc Natl Acad
744 Sci USA 113:2720–2725.

745 23. Li J, McQuade T, Siemer AB, Napetschnig J, Moriwaki K, Hsiao Y-S, Damko E, Moquin D, Walz T,
746 McDermott A, Ka-Ming Chan F, Wu H. 2012. The RIP1/RIP3 Necrosome Forms a Functional
747 Amyloid Signaling Complex Required for Programmed Necrosis. Cell 150:339–350.

748 24. Kleino A, Ramia NF, Bozkurt G, Shen Y, Nailwal H, Huang J, Napetschnig J, Gangloff M, Chan FK-
749 M, Wu H, Li J, Silverman N. 2017. Peptidoglycan-Sensing Receptors Trigger the Formation of
750 Functional Amyloids of the Adaptor Protein Imd to Initiate Drosophila NF-κB Signaling. Immunity
751 47:635-647.e6.

752 25. Mompeán M, Li W, Li J, Laage S, Siemer AB, Bozkurt G, Wu H, McDermott AE. 2018. The Structure
753 of the Necrosome RIPK1-RIPK3 Core, a Human Hetero-Amyloid Signaling Complex. Cell 173:1244-
754 1253.e10.

755 26. Beisson-Schecroun J. 1962. [Cellular incompatibility and nucleo-cytoplasmic interactions in the
756 "barrage" phenomena in Podospora anserina]. Ann Genet 4:4–50.

757 27. Balguerie A, Dos Reis S, Coulary-Salin B, Chaignepain S, Sabourin M, Schmitter J-M, Saupe SJ.
758 2004. The sequences appended to the amyloid core region of the HET-s prion protein determine
759 higher-order aggregate organization in vivo. J Cell Sci 117:2599–2610.

760 28. Beisson-Schecroun J. 1962. [Cellular incompatibility and nucleo-cytoplasmic interactions in the
761 "barrage" phenomena in Podospora anserina]. Ann Genet 4:4–50.

762 29. Benkemoun L, Ness F, Sabaté R, Ceschin J, Breton A, Clavé C, Saupe SJ. 2011. Two structurally
763 similar fungal prions efficiently cross-seed in vivo but form distinct polymers when coexpressed.
764 Mol Microbiol 82:1392–1405.

765 30. Nanson JD, Kobe B, Ve T. 2019. Death, TIR, and RHIM: Self-assembling domains involved in innate
766 immunity and cell-death signaling. J Leukoc Biol 105:363–375.

767 31. Kagan JC, Magupalli VG, Wu H. 2014. SMOCs: supramolecular organizing centres that control
768 innate immunity. Nat Rev Immunol 14:821–826.

769 32. Wu H. 2013. Higher-order assemblies in a new paradigm of signal transduction. Cell 153:287–
770 292.

771 33. Cai X, Chen ZJ. 2014. Prion-like polymerization as a signaling mechanism. Trends Immunol
772 35:622–630.

773 34. Dyrka W, Coustou V, Daskalov A, Lends A, Bardin T, Berbon M, Kauffmann B, Blancard C, Salin B,
774 Loquet A, Saupe SJ. 2020. Identification of NLR-associated amyloid signaling motifs in filamentous
775 bacteria. bioRxiv 2020.01.06.895854.

776 35. Burdett H, Bentham AR, Williams SJ, Dodds PN, Anderson PA, Banfield MJ, Kobe B. 2019. The
777 Plant "Resistosome": Structural Insights into Immune Signaling. Cell Host & Microbe 26:193–201.

778 36. Hofmann K. 2019. The Evolutionary Origins of Programmed Cell Death Signaling. Cold Spring Harb
779 Perspect Biol a036442.

780 37. Daskalov A, Saupe SJ. 2015. As a toxin dies a prion comes to life: A tentative natural history of
781 the [Het-s] prion. Prion 9:184–189.

782 38. Baker MODG, Shanmugam N, Pham CLL, Strange M, Steain M, Sunde M. 2018. RHIM-based
783 protein:protein interactions in microbial defence against programmed cell death by necroptosis.
784 Seminars in Cell & Developmental Biology https://doi.org/10.1016/j.semcdb.2018.05.004.

785 39. Plumley JA, Dannenberg JJ. 2010. The importance of hydrogen bonding between the glutamine
786 side chains to the formation of amyloid VQIVYK parallel beta-sheets: an ONIOM DFT/AM1 study.
787 J Am Chem Soc 132:1758–1759.

788 40. Halfmann R, Alberti S, Krishnan R, Lyle N, O'Donnell CW, King OD, Berger B, Pappu RV, Lindquist
789 S. 2011. Opposing effects of glutamine and asparagine govern prion formation by intrinsically
790 disordered proteins. Mol Cell 43:72–84.

791 41. Tuttle MD, Comellas G, Nieuwkoop AJ, Covell DJ, Berthold DA, Kloepper KD, Courtney JM, Kim JK,
792 Barclay AM, Kendall A, Wan W, Stubbs G, Schwieters CD, Lee VMY, George JM, Rienstra CM.
793 2016. Solid-state NMR structure of a pathogenic fibril of full-length human α-synuclein. Nat
794 Struct Mol Biol 23:409–415.

795 42. Lamacchia M, Dyrka W, Breton A, Saupe SJ, Paoletti M. 2016. Overlapping Podospora anserina
796 Transcriptional Responses to Bacterial and Fungal Non Self Indicate a Multilayered Innate
797 Immune Response. Front Microbiol 7:471.

798 43. Bergès T, Barreau C. 1989. Heat shock at an elevated temperature improves transformation
799 efficiency of protoplasts from Podospora anserina. J Gen Microbiol 135:601–604.

800 44. Benkemoun L, Sabaté R, Malato L, Dos Reis S, Dalstra H, Saupe SJ, Maddelein M-L. 2006. Methods
801 for the in vivo and in vitro analysis of [Het-s] prion infectivity. Methods 39:61–67.

802 45. Dos Reis S, Coulary-Salin B, Forge V, Lascu I, Bégueret J, Saupe SJ. 2002. The HET-s prion protein
803 of the filamentous fungus Podospora anserina aggregates in vitro into amyloid-like fibrils. J Biol
804 Chem 277:5703–5706.

805

806 **Table 1. Rate of spontaneous and induced prion formation and propagation**

transgenes	total moni-tored	spontaneous prion formation, days after transfection: 5			11			19			induced prion formation		
		diffuse	foci		diffuse	foci		diffuse	foci		diffuse	foci	
	n	n	n	%	n	n	%	n	n	%	n	n	%
HELLP(214-271)-RFP	34	27	7	21	13	21	62	2	32	94	0	24	100
HELLP(214-271)-GFP	47	40	7	15	24	23	49	8	39	83	0	24	100
GFP-HELLP(214-271)	33	11	22	67	1	32	97	0	33	100	0	24	100
RIP3(444-469)-RFP	39	18	21	54	8	31	80	2	37	95	0	24	100
RIP3(444-469)-GFP	46	30	16	35	15	31	67	4	42	91	0	24	100
GFP-RIP3(524-551)	25	8	17	68	3	22	88	0	25	100	0	24	100
RIP1(524-551)-RFP	26	23	3	12	14	12	46	10	16	62	0	24	100
RIP1(524-551)-GFP	27	27	0	0	25	2	7	23	4	15	0	24	100
GFP-RIP1(524-551)	38	38	0	0	36	2	5	35	3	8	0	24	100
PNT1(1-31)-GFP	25	18	7	28				1	24	96	0	24	100
PNT1(1-31)-RFP	25	17	8	32				0	25	100	0	24	100

807 For each transgene between 25 to 47 different transformants were monitored by fluorescence
808 microscopy for foci formation during 19 days. After 60 days 100% of the transformants (except RIP1-
809 GFP (33 %) and GFP-RIP1 (16%)) displayed dots. At least two other transformation experiments were
810 achieved for each transgene and generated 100% of tested transformants (n>10) with foci in
811 fluorescence after 60 days except for RIP1-GFP (20%) and GFP-RIP1 (15%).

812

Table 2. Growth alteration of strains co-expressing HELLP, CgHELLP or HET-S cell death inducing proteins and different prion forming domains prior and after prion infection.

co-expressed transgenes (PFD/cell-death inducer)	transfor-mants analyzed (n)	growth before infection								growth after infection							
		normal		altered		sub-lethal		total abnormal		normal		altered		sub-lethal		total abnormal	
		n	%	n	%	n	%	n	%	n	%	n	%	n	%	n	%
GFP-RIP3(444-469)/ HELLP-RFP	15	14	93	1	7	0	0	1	7	3	20	9	60	3	20	12	80
RIP3(444-469)-RFP/ HELLP-GFP	29	26	90	2	7	1	3	3	10	5	17	17	59	7	24	24	83
GFP-RIP3(444-469)/ HET-S-RFP	18	16	89	1	6	1	6	2	11	15	83	2	11	1	6	3	17
RIP3(444-469)-RFP/ HET-S-GFP	20	18	90	2	10	0	0	2	10	17	85	2	10	1	5	3	15
GFP-RIP1(524-551))/ HELLP-RFP	36	31	86	3	8	2	6	5	14	7	19	20	56	9	25	29	81
RIP3(444-469)-RFP/ HELLP-GFP	30	27	90	2	7	1	3	3	10	6	20	18	60	6	20	24	80
GFP-RIP1(524-551))/ HET-S-RFP	18	16	89	1	6	1	6	2	11	15	83	3	17	0	0	3	17
RIP1(524-551)-RFP/ HET-S-GFP	16	15	94	1	6	0	0	1	6	14	88	2	13	0	0	2	13
GFP(RIP3(444-459)/ CgHELLP-RFP	39	35	90	4	10	0	0	4	10	6	15	22	56	11	28	33	85
GFP-RIP1(524-551)/ HELLP-RFP	27	24	89	3	11	0	0	3	11	5	19	16	59	6	22	22	81
GFP-HELLP(214-271)/ HELLP-GFP	18	15	83	2	11	1	6	3	17	3	17	10	56	5	28	15	83
HELLP(214-271)-RFP/ HELLP-GFP	12	10	83	1	8	1	8	2	17	2	17	6	50	4	33	10	83
GFP-HELLF(209-277)/ HELLP-RFP	34	31	91	1	3	1	3	2	6	28	82	3	9	3	9	6	18
HELLF(209-277)-RFP/ HELLP-GFP	16	14	87	1	6	1	6	2	13	13	81	2	13	1	6	3	19
HET-s-RFP / HELLP-GFP	16	15	94	0	0	1	6	1	6	14	88	1	6	1	6	2	13

FIGURES

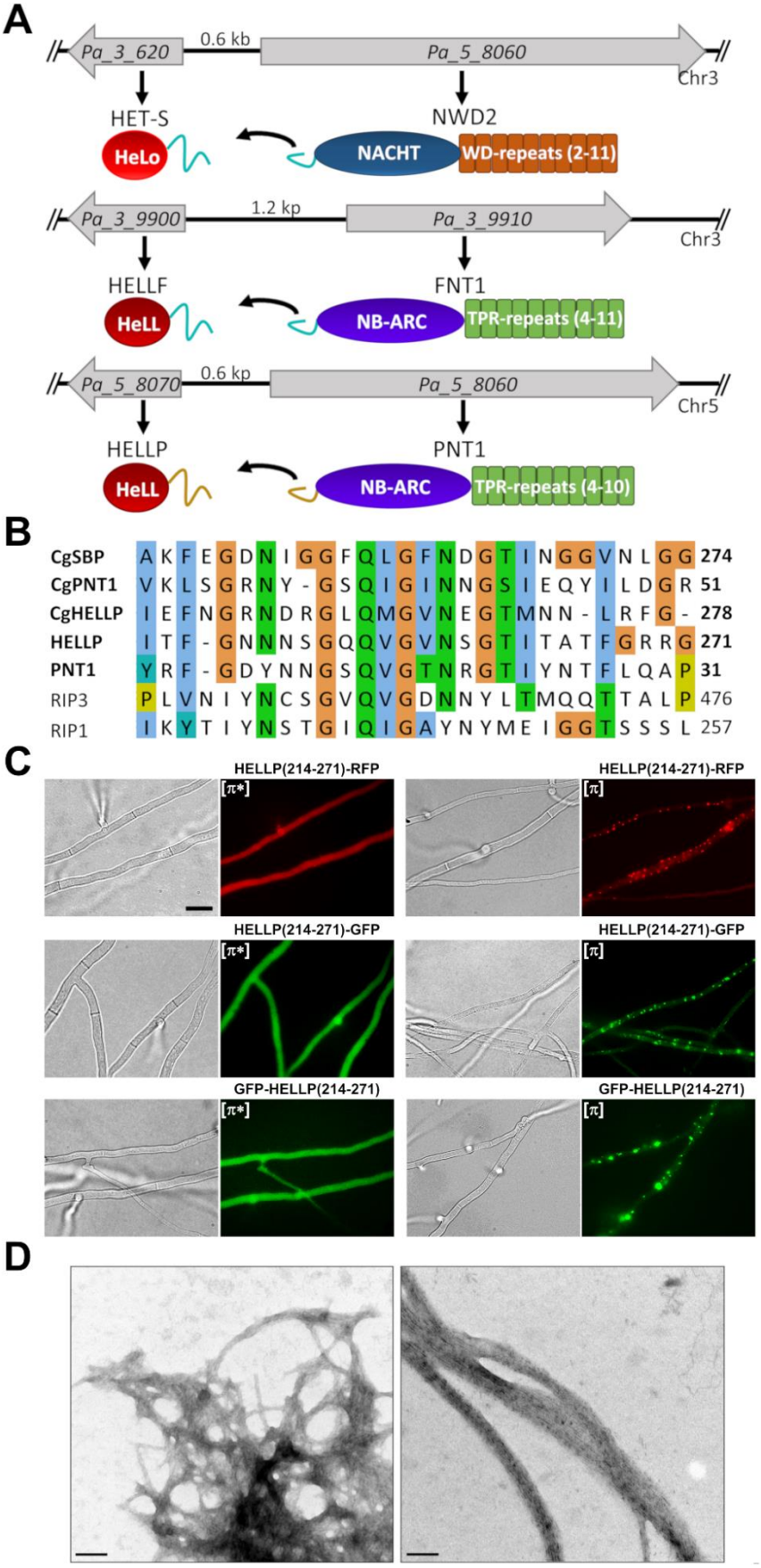
A
Pa_3_620
0.6 kb
Pa_5_8060
Chr3
HET-S
NWD2
HeLo
NACHT
WD-repeats (2-11)
Pa_3_9900
1.2 kp
Pa_3_9910
Chr3
HELLF
FNT1
HeLL
NB-ARC
TPR-repeats (4-11)
Pa_5_8070
0.6 kp
Pa_5_8060
Chr5
HELLP
PNT1
HeLL
NB-ARC
TPR-repeats (4-10)
B
CgSBP A K F E G D N I G G F Q L G F N D G T I N G G V N L G G 274
CgPNT1 V K L S G R N Y - G S Q I G I N N G S I E Q Y I L D G R 51
CgHELLP I E F N G R N D R G L Q M G V N E G T M N N - L R F G - 278
HELLP I T F - G N N N S G Q Q V G V N S G T I T A T F G R R G 271
PNT1 Y R F - G D Y N N G S Q V G T N R G T I Y N T F L Q A P 31
RIP3 P L V N I Y N C S G V Q V G D N N Y L T M Q Q T T A L P 476
RIP1 I K Y T I Y N S T G I Q I G A Y N Y M E I G G T S S S L 257
C
HELLP(214-271)-RFP
[π*]
HELLP(214-271)-RFP
[π]
HELLP(214-271)-GFP
[π*]
HELLP(214-271)-GFP
[π]
GFP-HELLP(214-271)
[π*]
GFP-HELLP(214-271)
[π]
D

819 **Fig 1. Characterization of the PP motif of *P. anserina.***

820 (A) Genome organization and domain architecture of the *het-s/nwd2*, *hellf/fnt1* and
821 *hellp/pnt1* gene clusters of *P. anserina,* chromosome*,* gene orientation and intergenic
822 distances are given. These loci are composed of two adjacent genes encoding an effector
823 protein and a NLR receptor. The effector proteins are composed of a PFD and a HeLo or HELL
824 domain. The NLRs are composed of a PFD, a NB-ARC or NACHT nucleotide binding domain and
825 of WD or TPR repeats (repeat numbers are variable in wild-isolates as indicated). PFDs of the
826 HRAM family given in cyan and those of the PP family in light-brown line. (B) Alignment of the
827 PP motifs of HELLP, PNT1, CgHELLP, CgSBP, and CgPNT1 along with the RHIM motif of human
828 RIP1 and RIP3. (C) PP-motif region of HELLP behaves as a prion forming domain *in vivo* as
829 shown on micrographs of *P. anserina* strains expressing different molecular fusions
830 (HELLP(214-271-RFP/GFP, GFP-HELLP(214-271)) as indicated above each micrograph, (scale
831 bar is 5 µm). Transformants present initially a diffuse fluorescence in the non-prion state
832 designated [π*] (left) and systematically acquire dot-like fluorescent aggregates after contact
833 with a strain already expressing the infectious prion state designated [π] (right). (D) PP-motif
834 forms fibrils *in vitro* as shown on electron micrograph of negatively stained HELLP(214-271) fibrils,
835 (scale bar is 100 nm).

836

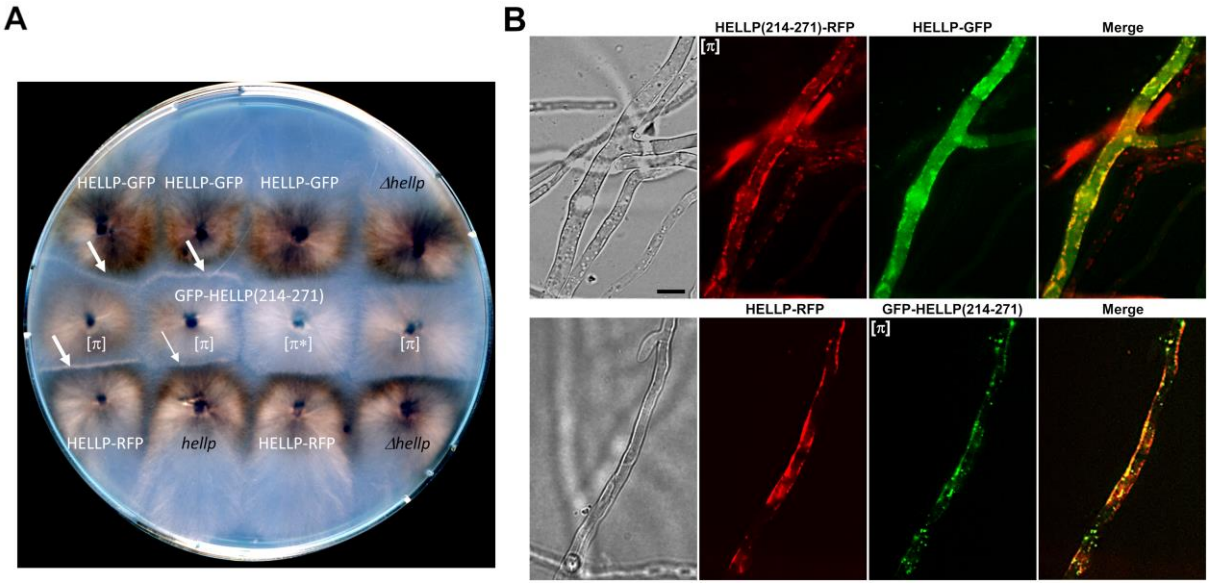

Fig 2. Activation of HELLP cell-death inducing activity by [π] prions.

(A) Observation of incompatibility reaction (barrage) between a strain containing [π] prions and expressing HELLP. Confrontation on solid medium of transformants expressing GFP-HELLP(214-271) in soluble [π*] or aggregated [π] states with strains expressing full-length HELLP from a transgene (labelled in white) or from the wild type *hellp* gene or with the *Δhellp* strain (both labelled in black). Barrages indicative of an incompatibility reaction, are marked by white arrows. The thinner arrow indicates an attenuated barrage reaction. (B) Micrographs of fusion cells co-expressing full-length HELLP (HELLP-GFP (upper panel) or HELLP-RFP (lower panel)), and HELLP(214-271)-RFP (upper panel) or GFP-HELLP(214-271) (lower panel) in the [π] aggregated state. Note that HELLP relocalizes to the cell membrane region in presence of [π], (scale bar is 5µm).

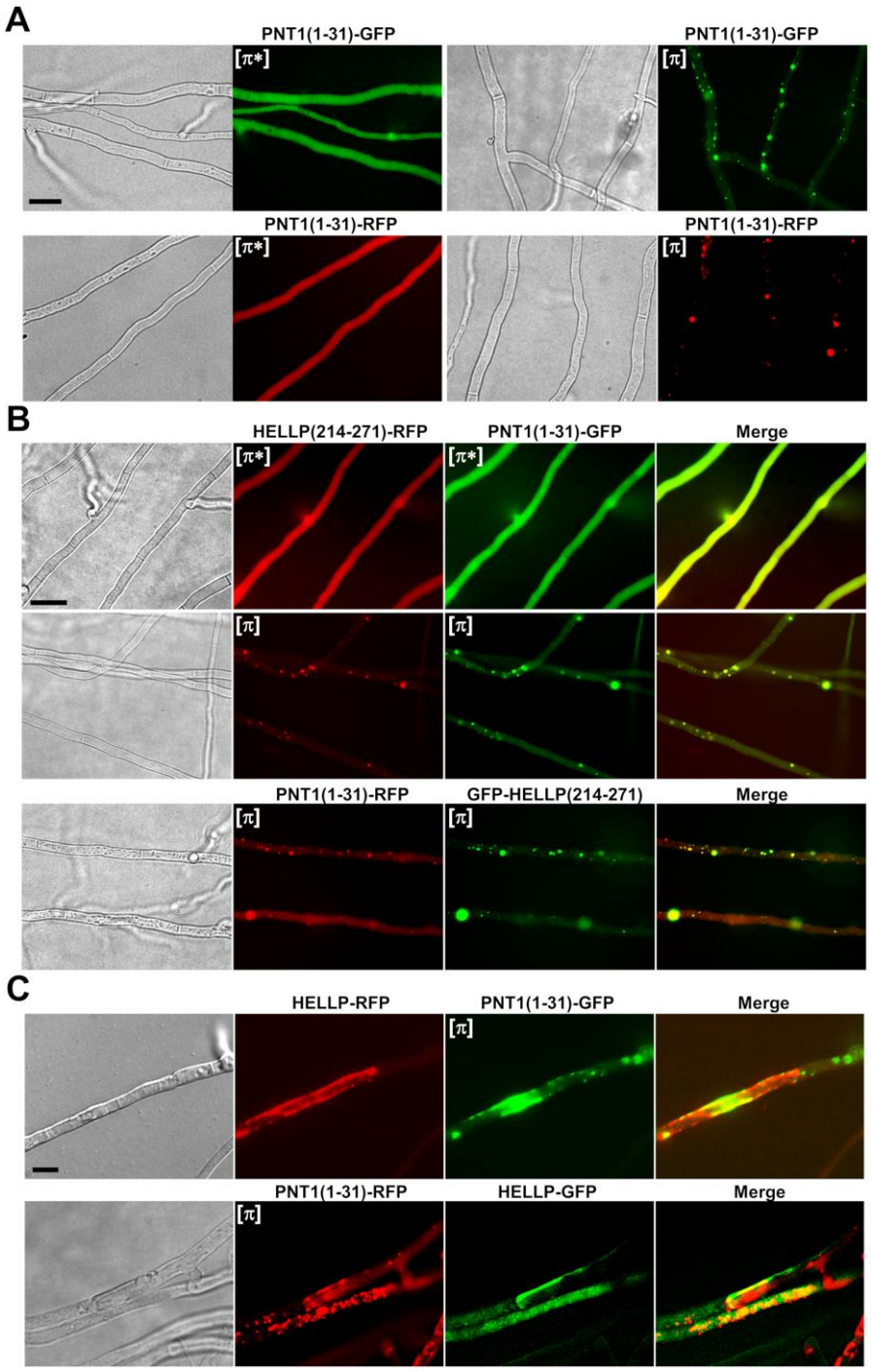

Fig 3. PNT1(1-31) forms [π] prions, co-localizes with HELLP(214-271) and induces toxicity of full-length HELLP

(A) Micrographs of PNT1(1-31) fusions with GFP or RFP either in the diffuse [π*] (left) or foci [π] state (right). (B) Micrographs showing co-localization of PNT1(1-31) and HELLP(214-271) in diffuse (top picture) or foci states. (C) In fusion cells co-expressing full-length HELLP (fused

856 with RFP (upper panel) or GFP (lower panel)), and foci forms of PaPNT1(1-31) (fused with GFP

857 (lower panel), or RFP, lower panel), HELLP relocalized to the plasma membrane region, (scale

858 bar is 2 μm).

859

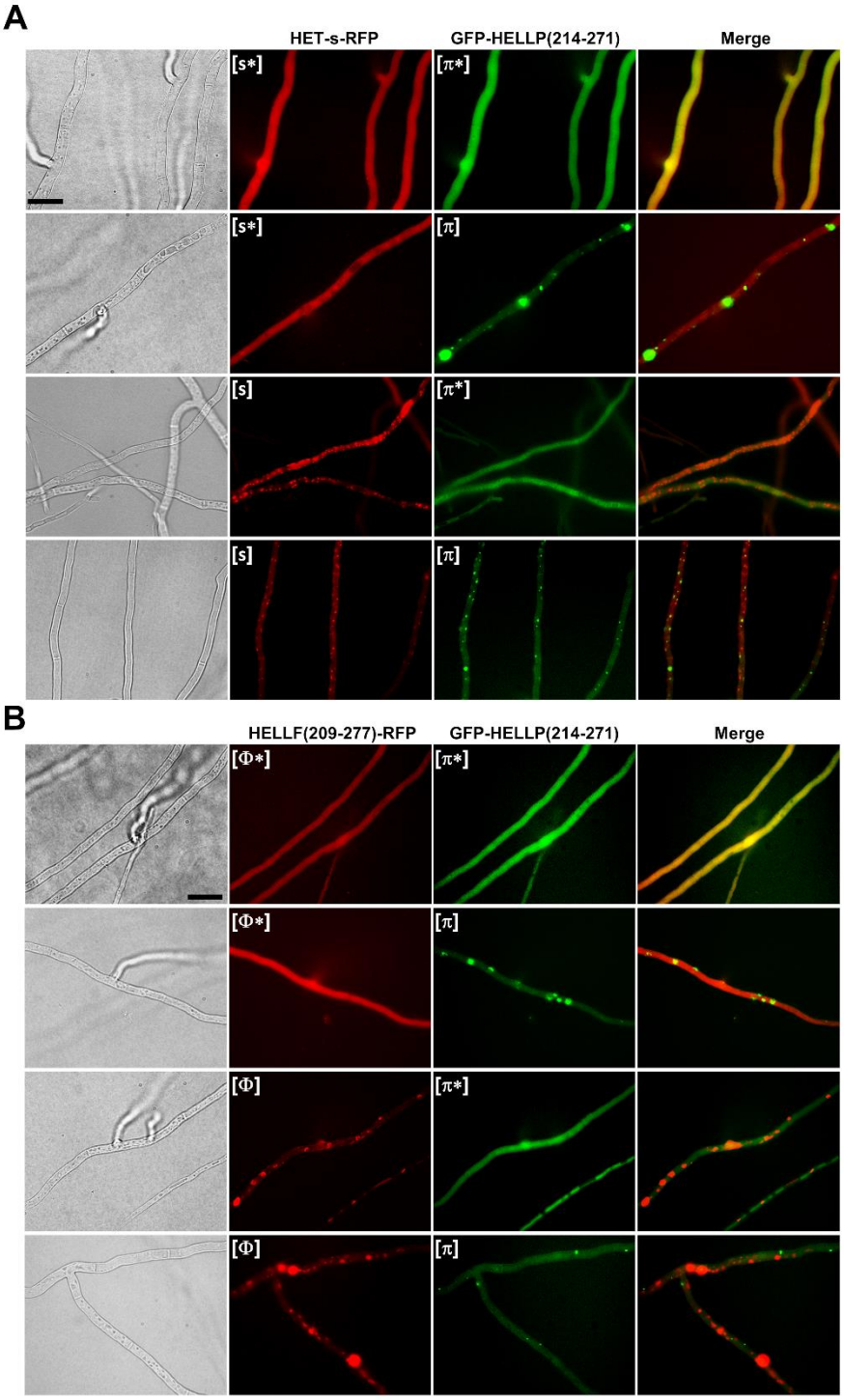

Fig 4. Lack of co-localization *in vivo* between [π] and [Het-s] or [Φ] prions.

(A) Micrographs of strains co-expressing HET-s-RFP ([Het-s] or [Het-s*] states, noted here [s*] and [s]) and GFP-HELLP(214-271) ([π*] or [π] state). Note an absence of co-localization of the prion forms and the independent occurrence of [π] and [Het-s], (scale bar is 5 μm). (B) Micrographs of strains co-expressing HELLF(209-277)-RFP ([Φ] or [Φ*] state) and GFP-

866 HELLP(214-271) ([π*] or [π] state). Note an absence of co-localization of the prion forms and

867 the independent occurrence of [π] and [Φ] (scale bar is 5 μm), (scale bar is 5 μm).

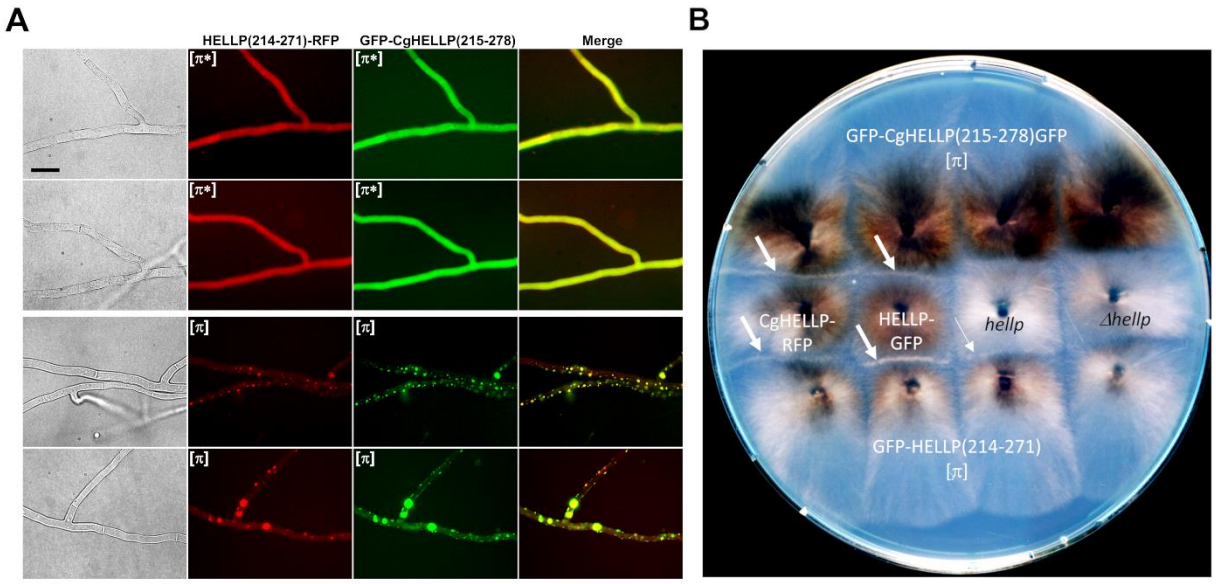

Fig 5. Co-localization of HELLP and CgHELLP PFDs and cross induction of cell-death activity. (A) Micrographs of strains co-expressing HELLP(214-271)-RFP and GFP-CgHELLP(215-278) in diffuse [π*] state (upper panels) or foci [π] state (lower panels). Note the co-localization of the two prion forms, (scale bar is 5 μm). (B) Confrontation on solid medium of strains expressing GFP-HELLP(214-271) and GFP-CgHELLP(215-278) [π] prions with strains expressing full-length HELLP from a transgene (marked in white) or from the wild type *hellp* gene or with the *Δhellp* strain (both marked in black). Barrages indicative of an incompatibility reaction, are marked by a white arrow. The thinner arrow indicates an attenuated barrage reaction.

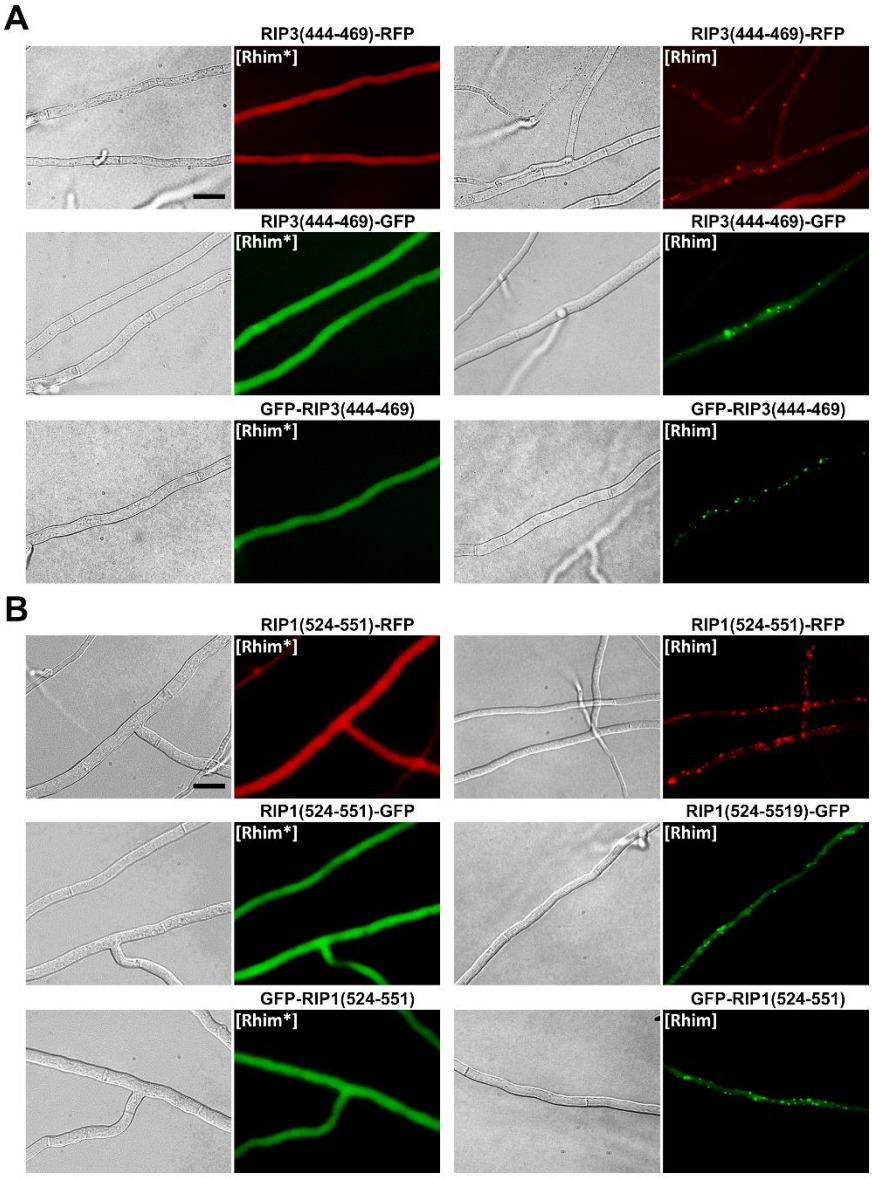

Fig 6. *In vivo* prion propagation of the human RIP3 and RIP1 RHIM regions in *Podospora anserina*.

(A) Micrographs of *P. anserina* strains expressing the RIP3(444-469)-RFP, RIP3(444-469)-GFP or GFP-RIP3(444-469) molecular fusions in the diffuse ([Rhim*]) and foci state ([Rhim]), (scale bar is 5 μm). (B) Micrographs of *P. anserina* strains expressing the RIP1(524-551)-RFP, RIP1(524-551)-GFP or GFP-RIP1(524-551)molecular fusions in the diffuse ([Rhim*]) and foci state ([Rhim]), (scale bar is 5 μm).

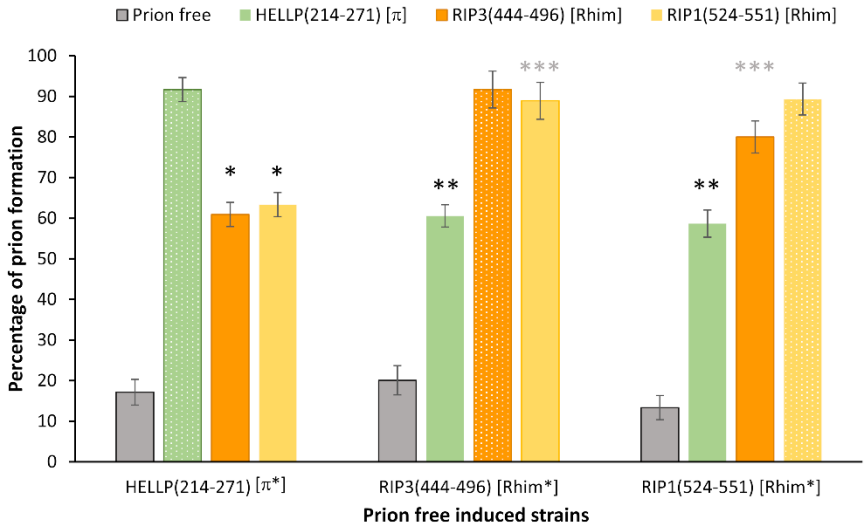

887

888 **Fig 7. Cross conversion between HELLP(214-271) [π] and [Rhim] prions.**

889 Histograms representing the percentage of [π] and [Rhim] prion containing strains obtained
890 after contact of recipient strains (initially displaying [π*] or [Rhim*] phenotype) with a
891 *Δhellp Δhet-s Δhellf* prion-free strain (control), a GFP-HELLP(214-271) [π] strain or GFP-
892 RIP3(444-469) or GFP-RIP1(524-551) [Rhim] strains (as indicated on top). Phenotype after
893 induction was determined by monitoring the acquisition of foci by fluorescence microscopy.
894 Percentages of prion formation were expressed as the mean value ± standard deviation on 4
895 distinct transformants for each genotype (resulting in 56 to 108 independent infections per
896 genotype). Homotypic inductions are showed with striped lines. P-values for cross conversion
897 were determined using two tails Fisher's test by comparison of the number of prion free and
898 prion containing strains obtained after induction by the prion free control or by the
899 heterotypic prion containing strain, (*: p-values $<10^{-8}$, **: p-values $<10^{-12}$).

900

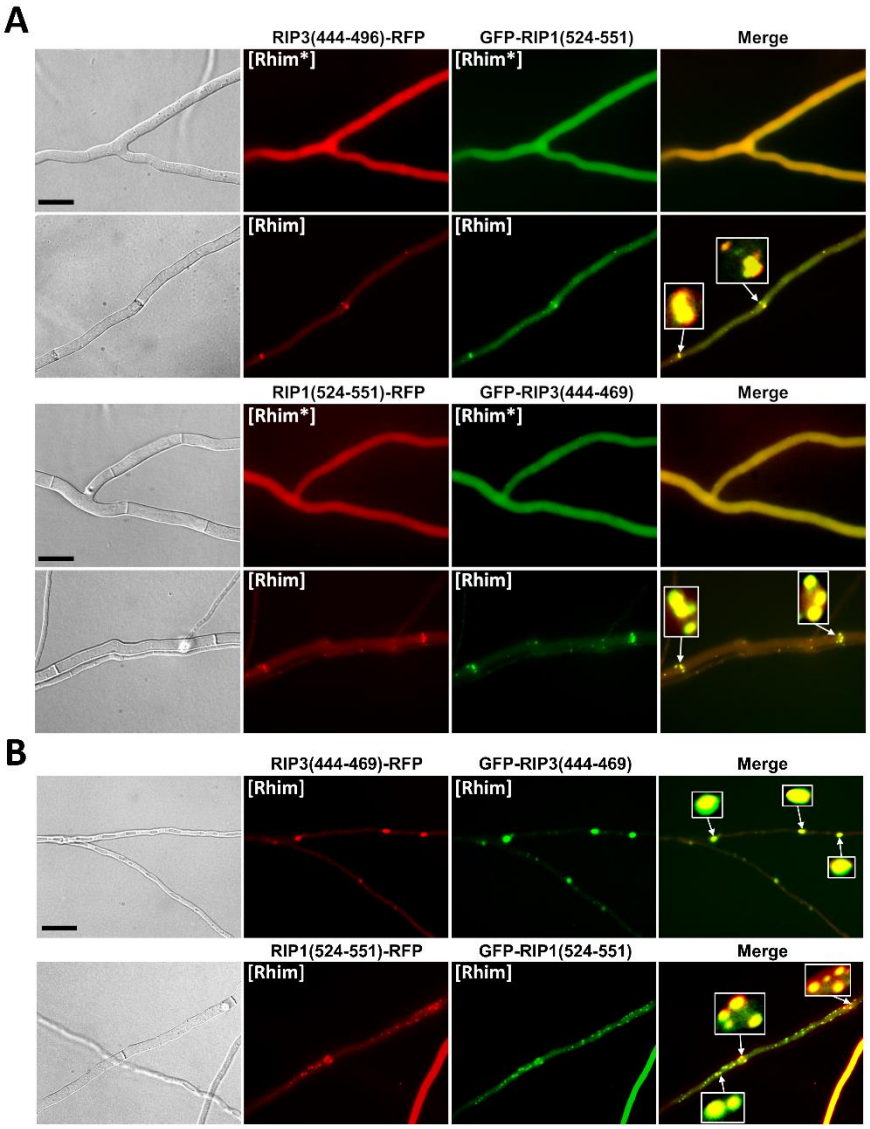

Fig 8. Co-localization of RIP1(524-551) and RIP3(444-469) foci in *Podospora anserina*.

(A) Micrographs of *P. anserina* strains co-expressing the RIP3(444-469)-RFP and GFP-RIP1(524-551) or GFP-RIP3(444-469) and RIP1(524-551)-RFP molecular fusions, (scale bar is 5 µm). Note the strong co-localization between [Rhim] foci and dots alignment close to the septa (zoomed regions). (B) Micrographs of strains co-expressing GFP-RIP3(444-469) and RIP3(444-469)-RFP or GFP-RIP1(524-551) and RIP1(524-551)-RFP of [Rhim] phenotypes. Note the almost complete overlapping of foci of [Rhim] homopolymers, (scale bar is 5 µm).

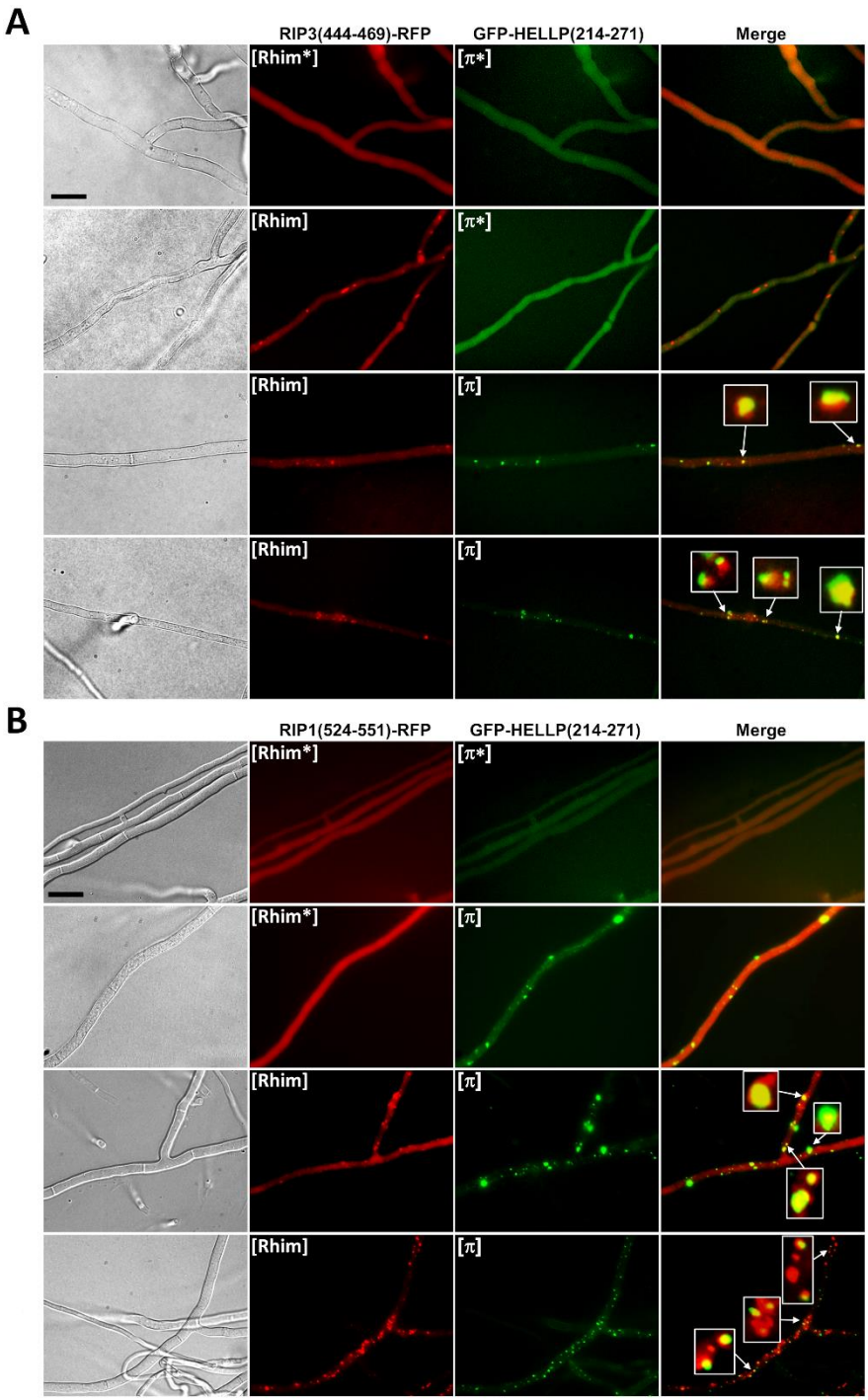

Fig 9. Partial co-localization of [π] and [Rhim] prions.

(A) Micrographs of strains co-expressing RIP3(444-469)-RFP ([Rhim*] or [Rhim] states) and GFP-HELLP(214-271) ([π*] or [π] states). (B) Micrographs of strains co-expressing RIP1(524-551)-RFP ([Rhim*] or [Rhim] states) and GFP-HELLP(214-271) ([π*] or [π] states). In both cases, note the co-existence in the second lane of [Rhim] and [π*] (A) or [Rhim*] and [π] (B), these

916 situations are only observable for a short period of time and upon prolonged subculture both
917 prion forms occur together. Note also the partial co-localization of the two prions, some of
918 the dots were zoomed to show incomplete overlapping in foci, (scale bar is 5 µm).
919

After prion-infection

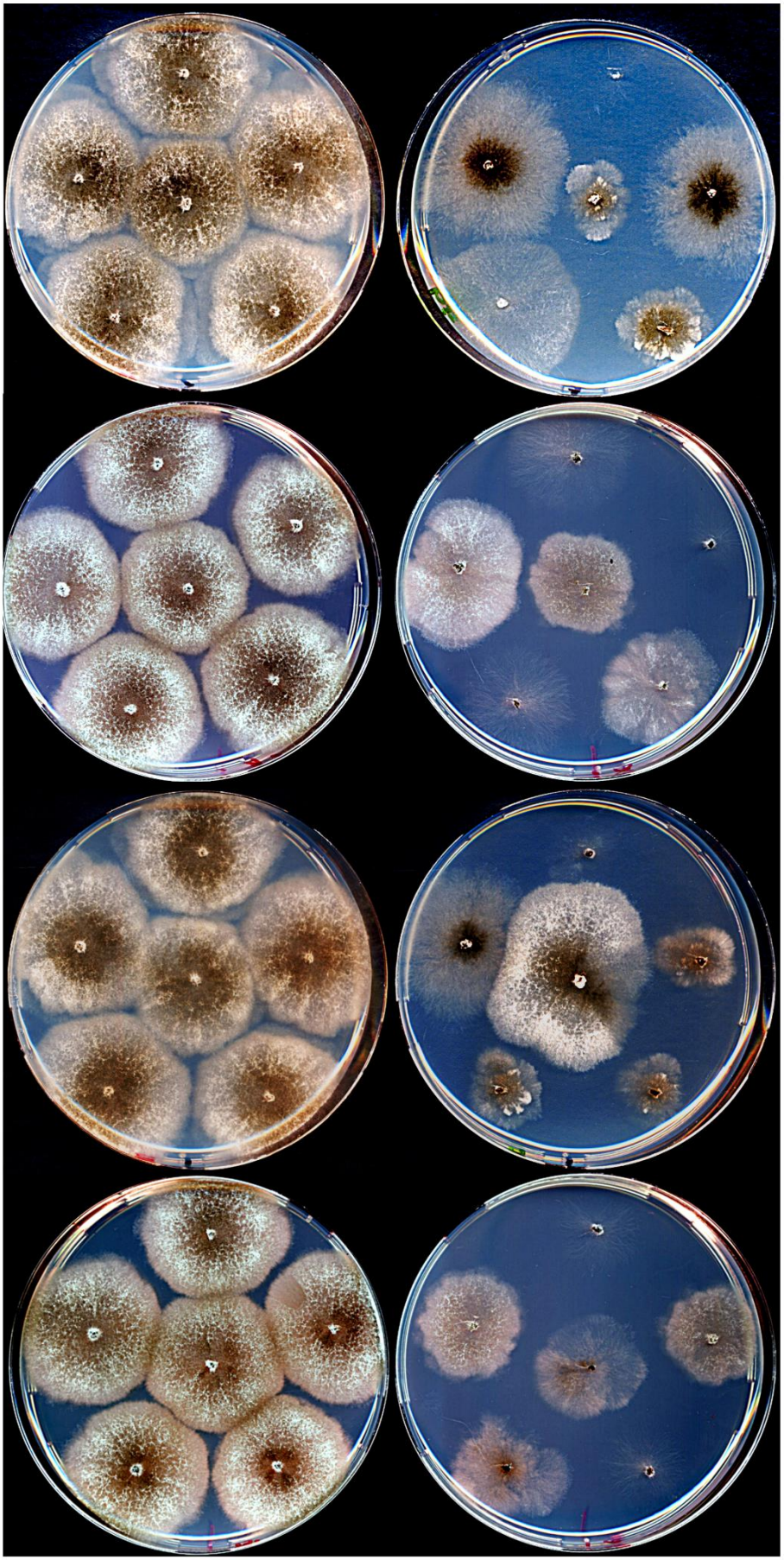

HELLP/
RHIM RIP1

HELLP/
RHIM RIP3

CgHELLP/
RHIM RIP1

CgHELLP/
RHIM RIP3

920

921 **Fig 10. [Rhim] prions elicit self-incompatibility in strains co-expressing HELLP or CgHELLP**

922 **and RIP1 or RIP3 RHIM**

923 Comparison of growth on solid medium of strains co-expressing HELLP-RFP (HELLP) or
924 CgHELLP-RFP (CgHELLP) and GFP-RIP1(524-551) (RIP1 RHIM) or GFP-RIP3(444-469) (RIP3
925 RHIM) before (left column) and after contact with a [Rhim] prion containing strain (right
926 column, after prion-infection). Note that infection with [Rhim] prions leads to self-
927 incompatibility with growth alterations ranging from a sublethal phenotype to a more or less
928 stunted growth.

929

Supporting information

Tables

Table S1. [π] prion propagation assayed in barrage tests.

tested strain (prion recipient)		previous contact with (prion donor)		tester strains		
				Δhellp Δhet-s Δhellf		recipient strain
recipient strain	transgene	recipient strain	transgene	HELLP-GFP	HELLP-RFP	transgene
Δhellp het-s°	GFP-HELLP (214-271) [π*]	*Δhellp het-s°*	no transgene	0/12	0/12	
			GFP-HELLP(214-271) [π]	12/12	12/12	
			HELLP (214-271)-GFP [π]	12/12	12/12	
			HELLP (214-271)-RFP [π*]	0/12	0/12	
			HELLP (214-271)-RFP [π]	12/12	12/12	
			HELLP (171-271)-GFP [π]	12/12	12/12	
			GFP-HELLP (171-271) [π]	12/12	12/12	

The table gives the number of transformants producing a barrage reaction (after contact with the given prion donor strain), to two different tester strains expressing full-length HELLP (either as GFP or RFP fusion). For each transgene, 12 different transformants were tested and the experiment done in triplicate. All triplicates were consistent.

939 **Table S2. Test of cross-conversion between [π]$^{PNT1(1-31)}$ and [π]$^{HELLP(214-271)}$ prions**

940

tested strain (prion recipient)		previous contact with (prion donor)		tester strains *Δhellp Δhet-s Δhellf*		recipient strain
recipient strain	transgene	recipient strain	transgene	HELLP-RFP	HELLP-GFP	transgene
Δhellp Δhet-s Δhellf	HELLP (214-271)-RFP [π*]	*Δhellp Δhet-s Δhellf*	PNT1(1-31)-GFP [π]	12/12	12/12	
			PNT1(1-31)-GFP [π*]	0/12	0/12	
			PNT1(1-31)-RFP [π]	12/12	12/12	
			PNT1(1-31)-RFP [π*]	0/12	0/12	
Δhellp Δhet-s Δhellf	PNT1(1-31)-RFP [π*]	*Δhellp Δhet-s Δhellf*	GFP-HELLP (214-271) [π]	12/12	12/12	

941 The table gives the number of transformants producing a barrage reaction (after contact with the given
942 prion donor strain), to two different tester strains expressing full-length HELLP (either as GFP or RFP
943 fusion). For each transgene, 12 different transformants were tested and the experiment done in
944 triplicate. All triplicates were consistent.

945 **Table S3. Assay in barrage tests of [π*] conversion by [Het-s] and [Φ] prions**
946

tested strain (prion recipient)		previous contact with (prion donor)		tester strains		
				Δhellp Δhet-s Δhellf		recipient strain
recipient strain	transgene	recipient strain	transgene	HELLP-RFP	HELLP-GFP	transgene
Δhellp Δhet-s Δhellf	HELLP (214-271)-GFP [π*]	*Δhellp Δhet-s Δhellf*	HET-s-RFP [Het-s]	0/12	0/12	
			GFP-HELLF(209-277) [Φ]	0/12	0/12	
			GFP-HELLP (214-271) [π]	12/12	12/12	
Δhellp Δhet-s Δhellf	HELLP (214-271)-RFP [π*]	*Δhellp Δhet-s Δhellf*	HET-s-RFP [Het-s]	0/12	0/12	
			GFP-HELLF(209-277) [Φ]	0/12	0/12	
			GFP-HELLP (214-271) [π]	12/12	12/12	

947 The table gives the number of transformants producing a barrage reaction (after contact with the given
948 prion donor strain), to two different tester strains expressing full-length HELLP (either as GFP or RFP
949 fusion). For each transgene, 12 different transformants were tested and the experiment done in
950 triplicate. All triplicates were consistent.

951 **Table S4. Test of cross-induction of incompatibility between three *P. anserina* amyloid**

952 **signaling systems**

tested strains		tester strain			
		Δhellp Δhets Δhellf			recipient strain
recipient strain	transgene	HET-S-GFP	HELLF-GFP	HELLP-GFP	transgene
Δhellp Δhet-s Δhellf	HET-s-RFP	18/18	0/18	0/18	
Δhet-s	HET-s(218-289)-GFP	18/18*	0/18	0/18	
Δhellp Δhet-s Δhellf	HELLF(209-277)-RFP	0/18	18/18	0/18	
Δhellp Δhet-s Δhellf	GFP-HELLF(209-277)	0/18	18/18	0/18	
Δhellp Δhet-s Δhellf	HELLF(L52K)-GFP	0/18	18/18	0/18	
Δhellp Δhet-s Δhellf	HELLP(214-271)-GFP	0/18	0/18	18/18	
Δhellp Δhet-s Δhellf	GFP-HELLP(214-271)	0/18	0/18	18/18	
Δhellp het-s°	GFP-CgHELLP(215-278)	0/18	0/18	18/18	

953 The table gives the number of transformants producing a barrage reaction to the given tester strains.
954 For each transgene, 18 different transformants were tested and the experiment was done in triplicate.
955 All triplicate were consistent. *As noted previously, HET-s(218-289)-GFP produces an attenuated
956 barrage reaction to HET-S.

957

958

959 **Table S5. Test of cross-conversion between [π]^{Pa} and [π]^{Cg} prions and induction HELLP and**

960 **CgHELLP toxicity**

tested strain (prion recipient)		previous contact with (prion donor)		tester strains		
				Δhellp het-s°	*Δhellp Δhet-sΔhellf*	recipient strain
recipient strain	transgene	recipient strain	transgene	CgHELLP-RFP	HELLP-RFP	transgene
Δhellp Δhet-sΔhellf	GFP-HELLP (214-271) [π*]	*Δhellp Δhet-sΔhellf*	none	0/12	0/12	
		Δhellp Δhet-sΔhellf	GFP-HELLP (214-271) [π]	12/12	12/12	
		Δhellp het-s°	GFP-CgHELLP (215-278) [π]	12/12	12/12	
Δhellp het-s°	GFP-CgHELLP (215-278) [π*]	*Δhellp Δhet-sΔhellf*	none	0/12	0/12	
		Δhellp Δhet-sΔhellf	GFP-HELLP (214-271) [π]	12/12	12/12	
		Δhellp het-s°	GFP-CgHELLP (215-278) [π]	12/12	12/12	

961 The table gives the number of transformants producing a barrage reaction (after contact with the given
962 prion donor strain), to two different tester strains expressing either full-length HELLP-RFP or full-length
963 CgHELLP-RFP. For each transgene, 12 different transformants were tested and the experiment done in
964 triplicate. All triplicates were consistent.

965

966 **Table S6. Cross-induction of HELLP and CgHELLP cell death activity by [π] prions.**

967

tested strains		tester strains					recipient strain
		Δhellp Δhet-sΔhellf	*Δhellp Δhet-sΔhellf*	*Δhellp Δhet-sΔhellf*	*wt*	*Δhellp het-s°*	
Recipient strain	Transgene	none	HELLP-RFP	HELLP-GFP	none	CgHELLP -RFP	transgene
Δhellp Δhet-sΔhellf	none	0/18	0/18	0/18	0/18	0/18	
Δhellp Δhet-sΔhellf	GFP-HELLP (214-271)	0/18	18/18	18/18	18/18[a]	18/18	
Δhellp Δhet-sΔhellf	GFP-HELLP (171-271)	0/18	18/18	18/18	18/18[a]	18/18	
Δhellp Δhet-sΔhellf	HELLP (214-271)-RFP	0/18	18/18	18/18	18/18[a]	18/18	
Δhellp het-s°	GFP-CgHELLP (215-278)	0/18	18/18	18/18	0/18	18/18	
Δhellp het-s°	CgHELLP (170-278)-RFP	0/18	18/18	18/18	0/18	18/18	

968 The table gives the number of transformants producing a barrage reaction to the given tester strains
969 ([a] barrage was attenuated). For each transgene, 18 different transformants were tested and the
970 experiment was done in triplicate. All triplicates were consistent.

971

972

973 **Table S7. Occurrence of the different phenotypes observed using fluorescence microscopy**

974 **during co-expression experiments.**

co-expressed transgenes	phenotypes	independent observations	number of cells observed
HET-s HELLP(214-271)	[Het-s*] [π*]	30	148
	[Het-s] [π*]	14	124
	[Het-s*] [π]	31	132
	[Het-s] [π]	17	141
HELLF(209-277) HELLP(214-271)	[ϕ*] [π*]	18	85
	[ϕ] [π*]	13	68
	[ϕ*] [π]	17	87
	[ϕ] [π]	18	82
HELLP(214-271) CgHELLP(215-278)	[π*] [π*]	6	36
	[π] [π]	10	56
PNT1(1-31) HELLP(214-271)	[π*] [π*]	9	88
	[π] [π]	12	71
RIP3(444-469) RIP3(444-469)	[Rhim*] [Rhim*]	2	14
	[Rhim] [Rhim]	23	178
RIP3(444-469) RIP1(524-551)	[Rhim*] [Rhim*]	16	85
	[Rhim] [Rhim]	27	123
RIP3(4444-469) HELLP(214-271)	[Rhim*] [π*]	5	27
	[Rhim] [π*]	6	33
	[Rhim*] [π]	3	18
	[Rhim] [π]	32	170
RIP1(524-551) HELLP(214-271)	[Rhim*] [π*]	12	71
	[Rhim] [π*]	6	36
	[Rhim*] [π]	20	95
	[Rhim] [π]	10	48

975 Prion phenotypes are defined by presence of foci of the corresponding fusion protein.

976

977 **Table S8. Count of co-localized foci observed by fluorescence microscopy during co-**

978 **expression experiments.**

				number of dots			
				at least partially co-localized		not co-localized	
co-expressed transgenes	co-expressed prions	independent observations	number of cells observed	n	%	n	%
HET-s HELLP(214-271)	[Het-s] [π]	17	141	50	5.1	925	94.9
HELLF(209-277) HELLP(214-271)	[ϕ] [π]	18	82	33	4.7	663	95.3
HELLP(214-271) CgHELLP(215-278)	[π] [π]	10	56	428	90.5	45	9.5
PNT1(1-31) HELLP(214-271)	[π] [π]	12	71	222	94.1	14	5.9
RIP3(444-469) RIP3(444-469)	[Rhim] [Rhim]	23	178	524	96.0	22	4.0
RIP3(444-469) RIP1(524-551)	[Rhim] [Rhim]	27	123	462	82.1	101	17.9
RIP3(444-469) HELLP(214-271)	[Rhim] [π]	32	170	330	68.2*	154	31.8
RIP1(524-551) HELLP(214-271)	[Rhim] [π]	10	48	293	67.4*	142	32.6

979 Counts of co-localized dots correspond to counts of foci with perfect or partial superposition of GFP
980 and RFP whereas counts of not co-localized dots correspond to the number of isolated GFP dots plus
981 the number of isolated RFP dots. * p-values were determined using two tails Fisher's test by
982 comparison of the number of co-localized dots in [Rhim] / [π] co-expressions to the number of not co-
983 localized dots for non-cross interacting prion combination ([Het-s]/[π] or [ϕ]/[π]) and were $<10^{-10}$).
984

Supplementary figures

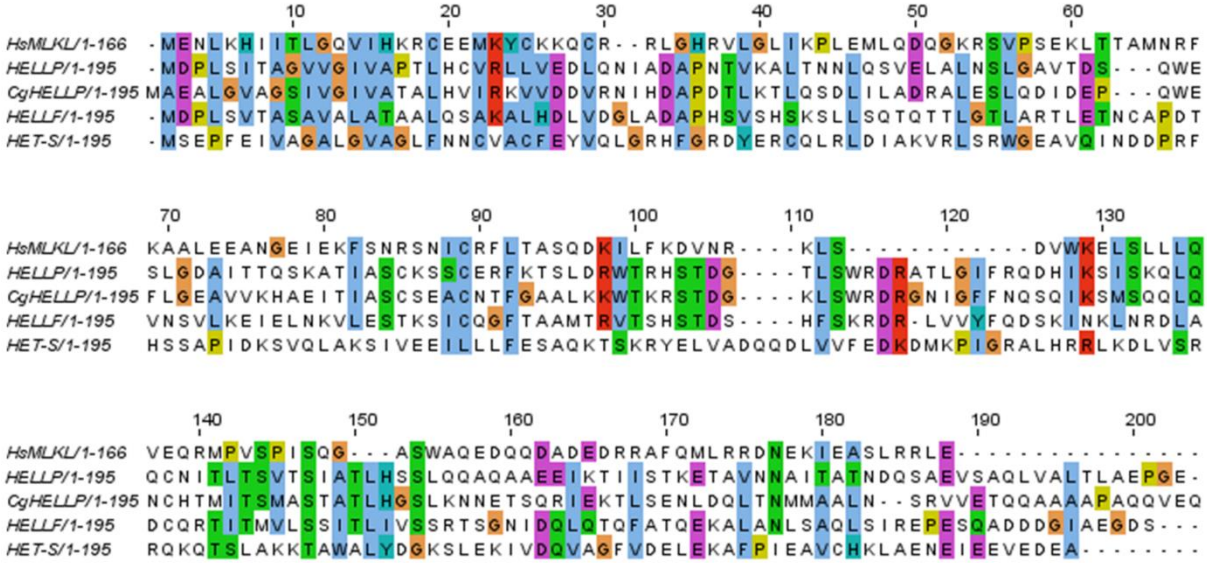

Fig S1. Homology between HeLo or HELL domains of *P. anserina* and 4HB domain of human MLKL.

Alignment of the HET-S HeLo domain and the HELLF and HELLP HELL domains of *P. anserina* with the 4HB region of the human MLKL. Alignment was generated with clustal omega with default settings.

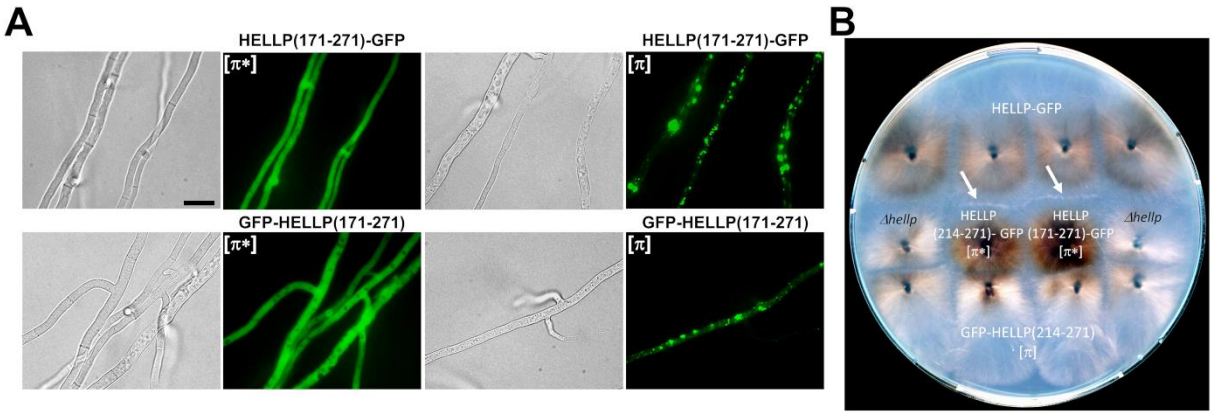

Fig S2. [π] prion propagation of longer HELLP constructs.

(A) Micrographs of *P. anserina* strains expressing HELLP(171-271)-GFP or GFP-HELLP(171-271) as indicated above each micrograph (scale bar is 5 µm). Transformants presenting a diffuse fluorescence in the non-prion state designated [π*] (left) and dot-like fluorescence after contact with a [π] strain (right). (B) Barrage tests showing conversion of [π*] strains (expressing either HELLP(214-271)-GFP or HELLP(171-271)-GFP) to the [π] phenotype by contact with strains expressing GFP-HELLP(214-271) in the [π] state.

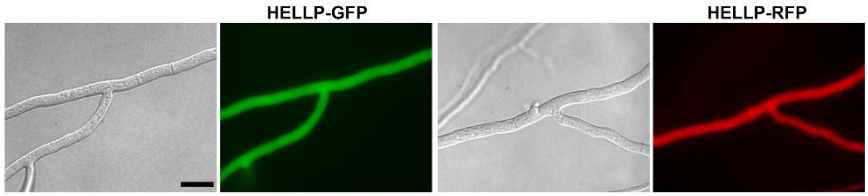

Fig S3. HELLP full-length diffuse and cytoplasmic localization.

Micrographs of strains expressing HELLP-GFP or HELLP-RFP fusion proteins. The fluorescence signal is diffuse and cytoplasmic and remains stable, (scale bar is 5µm).

1007 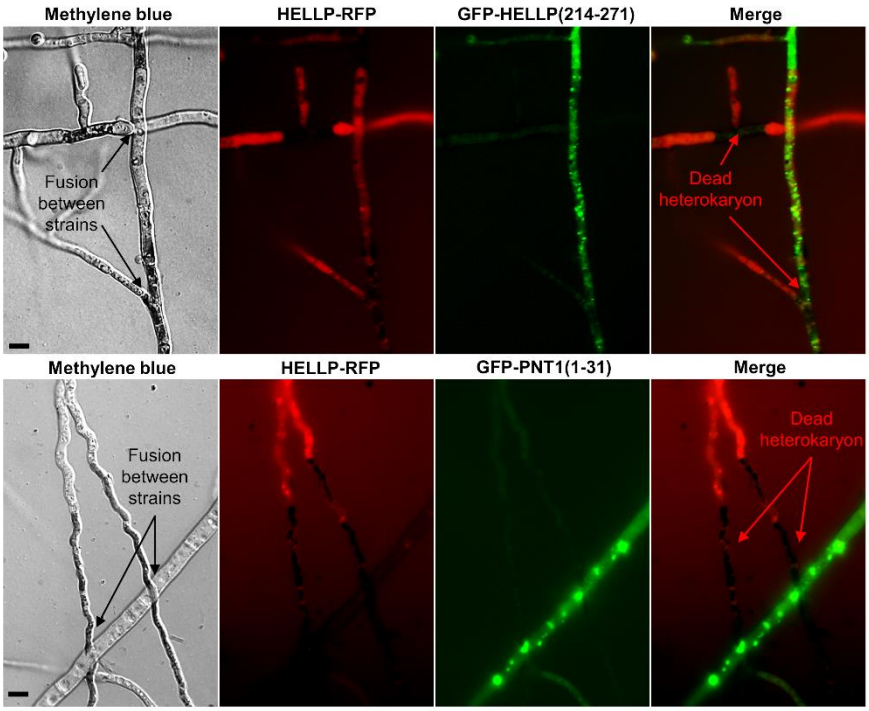

1008 **Fig S4. Death of fusion cells containing [π] prions and HELLP full-length proteins.**

1009 Micrographs showing contact zone between HELLP-RFP and GFP-HELLP(214-271) (Top panel)

1010 or GFP-PNT1(1-31) (Bottom panel) expressing strains after Methylene blue staining. Note that

1011 heterokaryotic fusion cells are stained (appeared in black) indicating their death, (scale bar is

1012 2 μm).

1013

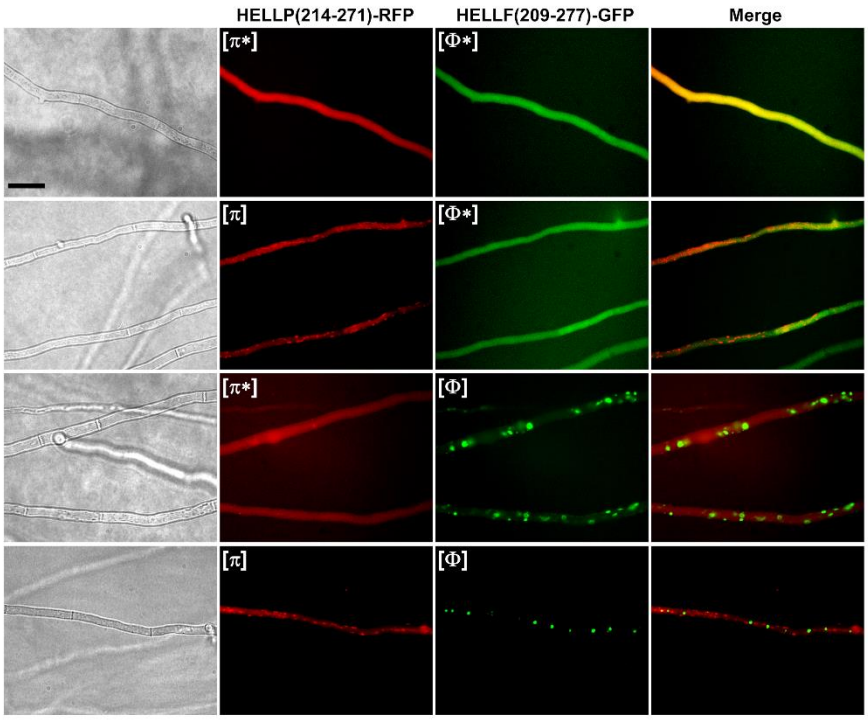

1014

1015 **Fig S5. Absence of co-localization HELLP(214-271)-RFP and HELLF(209-277)-GFP foci.**

1016 Micrographs of strains co-expressing HELLP(214-271)-RFP ([π*] or [π] state) and HELLF(209-

1017 277)-GFP ([Φ*] or [Φ] state). Note that HELLP(214-271)-RFP and HELLF(209-277)-GFP foci do

1018 not co-localize ([Φ] and [π]) and the existence of cells in which one of the fusion protein forms

1019 foci while the other remains diffuse, (scale bar is 5 μm).

1020

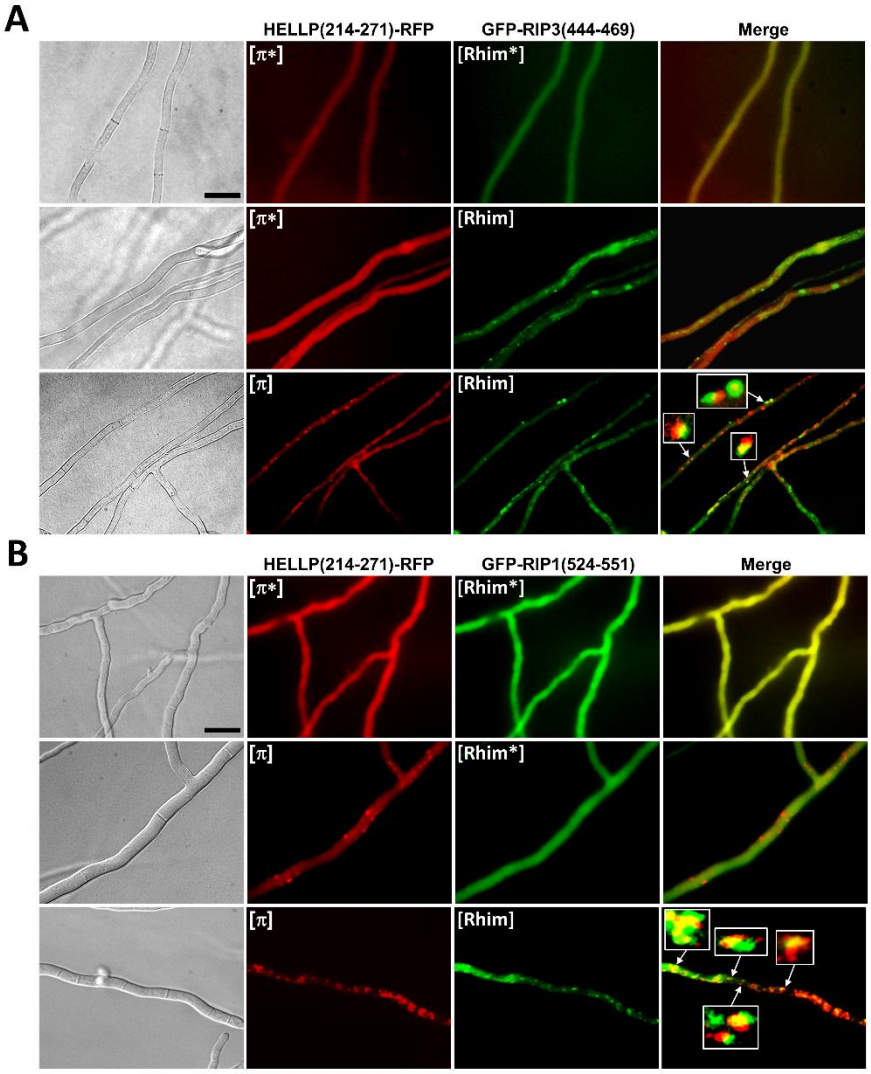

Fig S6. Partial co-localization HELLP(214-271)-RFP foci and GFP-RIP1(524-551) and GFP-RIP3(444-469) foci.

(A) Micrographs of strains co-expressing GFP-RIP3(444-469) ([Rhim*] or [Rhim] states) and HELLP(214-271)-RFP ([π*] or [π] states). (B) Micrographs of strains co-expressing GFP-RIP1(524-551) ([Rhim*] or [Rhim] states) and HELLP(214-271)-RFP ([π*] or [π] states). In both cases, note the co-existence on the second lane of [Rhim] and [π*] (A) or [Rhim*] and [π] (B),. Note the partial co-localization of the foci; some of the foci were magnified to show incomplete overlap of the fusion protein, (scale bar is 5 µm).

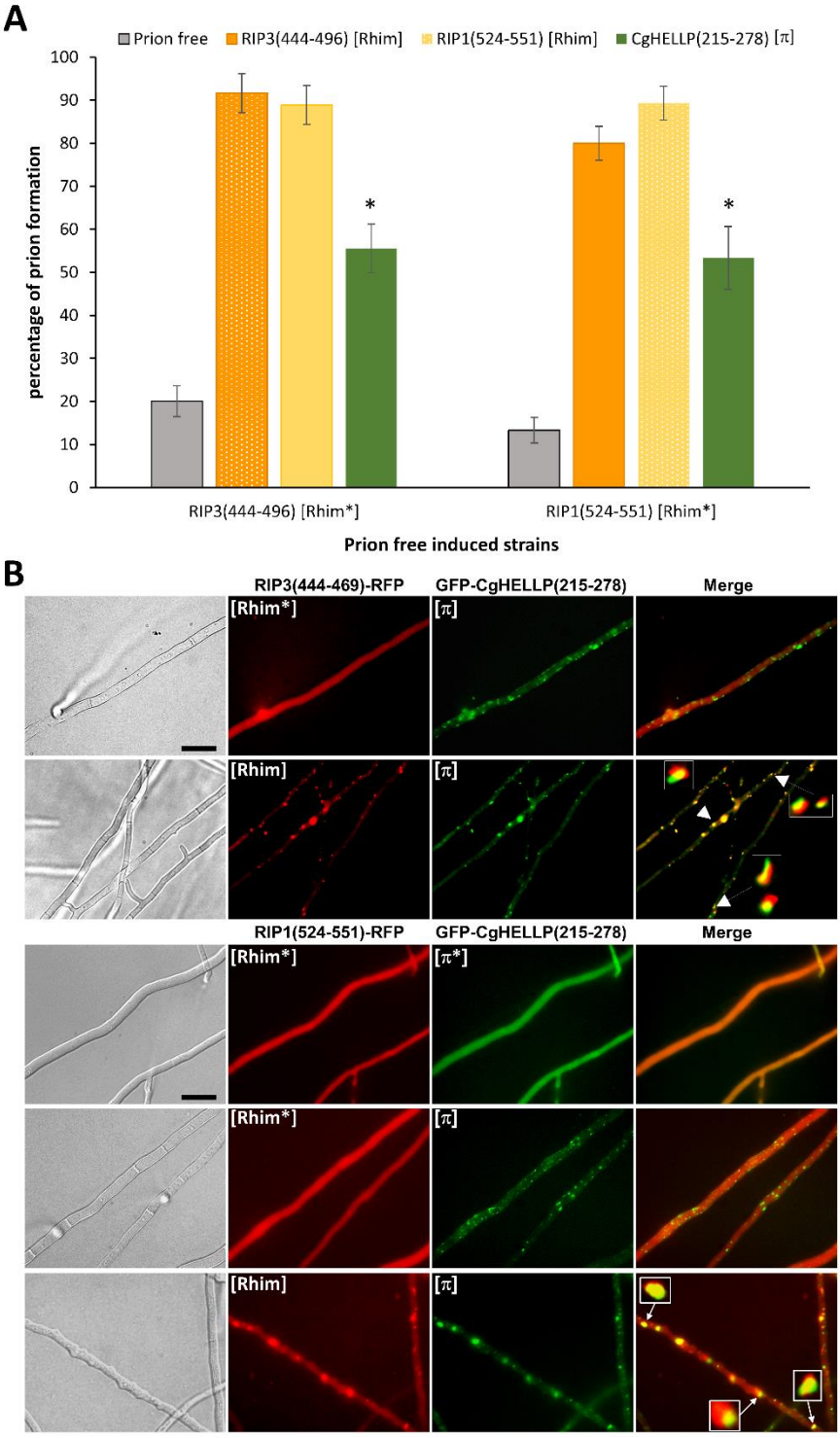

1032

1033 **Fig S7. Interaction between human RIP3 or RIP1 RHIM region and the CgHELLP PFD.**

1034 (A) Induction of [Rhim] prion by cross conversion of [Rhim*] by $[\pi]^{Cg}$ or [Rhim] prions.

1035 Histogram representing the percentage of [Rhim*] strains displaying [Rhim] phenotype after

1036 contact with a *Δhellp Δhet-s Δhellf* prion free strain (control), a GFP-CgHELLP(215-278) [π]

1037 containing strain or a GFP-RIP3(444-469) or GFP-RIP1(524-551) [Rhim] containing strains
1038 (indicated on top). Strains phenotype after induction was determined by monitoring the
1039 acquisition of dot-like aggregates by fluorescence microscopy. Homotypic interactions shown
1040 with striped lines. Percentages of prion formation were expressed as the mean value ±
1041 standard deviation for 3 to 5 independent experiments on 4 different transformants. P-values
1042 for cross conversion were determined using two tails Fisher's test by comparison of the
1043 number of prion free and prion containing strains obtained after induction by the prion free
1044 control or by the heterotypic prion containing strain and are $<10^{-8}$. (B) Partial co-localization
1045 of [π] Cg and [Rhim] prions *in vivo*. Micrographs of strains co-expressing RIP3(444-469)-RFP or
1046 RIP1(524-551)-RFP ([Rhim*] or [Rhim] states) and GFP-CgHELLP(215-278) ([π*] and [π] state).
1047 Note the co-existence of [Rhim*] and [π], this situation is only observable for a short period
1048 of time, showing a low conversion rate of [Rhim*] by [π] prion. Note the partial co-localization
1049 of the two prions, some of the dots were zoomed to show incomplete overlapping, (scale bar
1050 is 5 µm).
1051

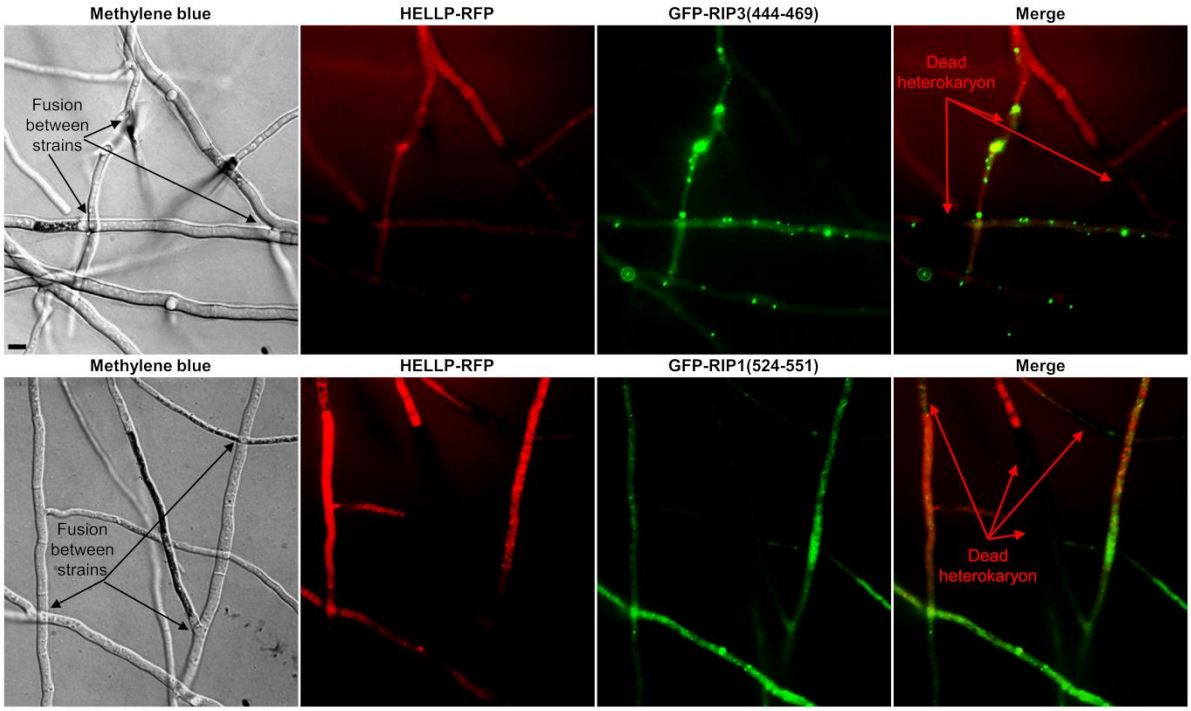

Fig S9. Cell death occurring in fusion cells between [Rhim] and HELLP expressing strains. Micrographs showing confrontations between HELLP-RFP and GFP-RIP3(444-469) (Upper panel) or GFP-RIP1(524-551) (lower panel) expressing strains after methylene blue staining. Note that heterokaryotic fusion cells are stained indicating their death, (scale bar is 2 μm).